

WIND TUNNEL INVESTIGATIONS AIMED AT DEVISING TESTS
OF AIRCRAFT SPIN

J. Gobeltz and M. Vanmansart

Translation of "Etudes en souffleries relatives à l'installation d'essais en vol de vrilles sur avions," Association Aéronautique et Astronautique de France, Colloque d'Aérodynamique Appliquée, 10th, Lille University, Lille, France, Nov. 7-9, 1973, Report, 42 pp.

(NASA-TT-F-15726) WIND TUNNEL
INVESTIGATIONS AIMED AT DEVISING TESTS OF
AIRCRAFT SPIN (Kanner (Leo) Associates)
50 p HC \$5.50
S/

CSCL 01A

3456789707

N74-27479

Unclas
42655
G3/01
JUN 1974
18152021222324252627

1. Report No. NASA TT F-15,726	2. Government Accession No.	3. Recipient's Catalog No.	
4. Title and Subtitle WIND TUNNEL INVESTIGATIONS AIMED AT DE- VISING TESTS OF AIRCRAFT SPIN		5. Report Date June 1974	
		6. Performing Organization Code	
7. Author(s) J. Gobeltz and M. Vanmansart, Lille University, Lille, France		8. Performing Organization Report No.	
		10. Work Unit No.	
9. Performing Organization Name and Address Leo Kanner Associates, P.O. Box 5187, Redwood City, California 94063		11. Contract or Grant No. NASW-2481	
		13. Type of Report and Period Covered Translation	
12. Sponsoring Agency Name and Address NATIONAL AERONAUTICS AND SPACE ADMINIS- TRATION, WASHINGTON, D.C. 20546		14. Sponsoring Agency Code	
15. Supplementary Notes Translation of "Etudes en souffleries relatives à l'instal- lation d'essais en vol de vrilles sur avions," Association Aéronautique et Astronautique de France, Colloque d'Aéro- dynamique Appliquée, 10th, Lille University, Lille, France, Nov. 7-9, 1973, Report, 42 pp.			
16. Abstract The nature and characteristics of and the conditions leading to aircraft spin are studied in a conventional and in a spin wind tunnel, using an anemometer technique adapted for this purpose. The results obtained provide better insight into the spin phenomenon and form a basis for developing means of recovering from spin. The use of a parachute and of auxiliary jets as a means of mastering aircraft spin is studied.			
17. Key Words (Selected by Author(s))		18. Distribution Statement Unclassified - Unlimited	
19. Security Classif. (of this report) Unclassified	20. Security Classif. (of this page) Unclassified	21. No. of Pages 48	22. Price

Table of Contents

	Page
Introduction	1
1. Anemometry adapted to spin	2
1.1. Device A	2
1.1.1. Description	2
1.1.2. Use	3
1.2. Device B	3
1.2.1. Operative principles	4
1.2.2. Information furnished by rod	5
1.2.3. Information furnished by ring	6
1.2.4. Utilization of measurements	9
1.2.5. Remarks	10
1.2.6. Vanes	11
1.2.7. Full-scale tests	12
2. Measurement of yawing moment	12
2.1. Preliminary remarks	12
2.2. Example of yawing moment at zero sideslip	13
2.3. Criteria for classification of modifications	14
2.3.1. Criterion of symmetrization	14
2.3.2. Criterion of stabilization	15
2.4. Modifications of nose	15
2.5. Effect of strakes on yawing moment	17
2.6. Relationship between yawing moment and anemometric measurements	17
3. Safety devices	19
3.1. Preliminary remarks	19
3.2. Parachutes	19
3.2.1. Principles of utilization	19
3.2.2. Results of wind tunnel parachute tests	20
3.3. Auxiliary surfaces	21
3.4. Rockets	22
3.4.1. Preliminary remarks	22
3.4.2. Results	23
3.4.2.1. Rocket influencing pitch	23
3.4.2.2. Rocket influencing yaw	23
3.4.2.3. Rocket influencing roll	24
3.4.2.4. Comparison of results obtained around three axes	24
3.4.3. Longitudinal action of a rocket	26
Figures	27

WIND TUNNEL INVESTIGATIONS AIMED AT DEVISING TESTS OF AIRCRAFT SPIN

J. Gobeltz and M. Vanmansart
Lille University, Lille, France

Introduction

/*

When the In-Flight Testing Centers were studying spin several decades ago, frequently these agencies had neither spin wind tunnel tests nor specially adapted instrumentation available to them, and in many cases the pilot's evaluation comprised the only usable information. Moreover, there were no safety means of recognized efficiency available to the pilot.

Subsequently, spin tests were conducted with mock-ups placed in a vertical wind tunnel, with a simultaneous attempt to make optimum use of the information furnished by conventional instrumentation.

Thus special instrumentation, especially from an anemometric standpoint, was found to be necessary in order to determine the real nature of the phenomena and to be able to analyze them.

The present article is based on recent research with the following objectives:

- to define an anemometric method adapted to spin and capable of supplying enough information to describe the phenomena correctly, even under highly disturbed conditions;
- to study safety devices appropriate for certain types of aircraft.

This research has yielded the following results:

*Since source pagination is not indicated in the original text, slashes in the margin indicate new page in the original.

- first, the nature of airflow around the nose of long-fuselage aircraft, showing how the shape of the nose influences the behavior of such aircraft during spin;
- and second, determination of a basis for research on suitable means of modifying the type of spin of a given aircraft or the spin control.

1. Anemometry Adapted to Spin

The first specialized anemometer (A) used for spin which will be discussed here is that described by Fromentel and Plessy in their paper presented to the AFITAE [Association Francaise des Ingénieurs et Techniciens de l'Aéronautique; French Association of Aeronautical Engineers and Technicians] in 1967. A review of the limitations of device A will be followed by a description of device B, which was studied recently, and whose capabilities are much higher.

1.1. Device A

1.1.1. Description

The anemometric device includes (see Fig. 1):

- a Chaffois rod secured along the forward axis of the fuselage (that is, $30^{\circ}30'$ dive) and including a total pressure gauge and two neighboring static pressure gauges, one termed the forward static gauge and the other the rear static gauge;
- a Badin total pressure gauge preset at 45° under the fuselage, within the plane of symmetry of the aircraft, its distance from the forward tip of the fuselage being equal to 80% of the mean chord of the wing;
- an incident vane under the nose;
- a sideslip vane on the right side of the nose.

The shafts of the vanes, normal to the skin of the nose, are

at a distance from the forward tip of the fuselage which is 30% of the mean chord of the wing.

1.1.2. Use

The operative principles of this anemometer are based on the simultaneous use of vanes and probes.

The sideslip vane makes it possible to choose a curve on the graph shown in Fig. 2 which gives a coefficient K making it possible to change from

Badin total pressure - Chaffois static pressure
to the kinetic pressure and, in addition, the incidence (this repeats the reading from the incident vane) as a function of the value of the ratio

$$\frac{\text{Chaffois total pressure} - \text{Chaffois static pressure}}{\text{Badin total pressure} - \text{Chaffois static pressure}}$$

This device could be used only at discrete points for relatively flat and disturbed spin, even if the disturbance was only moderate. This was due to the fact that the sideslip vane was attacked in a direction close to that of its axis of rotation. Figure 3 gives an example of a recording of the information furnished in this case by the sideslip vane. Obviously under such conditions only points of zero sideslip can be considered to furnish reliable data.

Moreover, the incident vane was masked for negative sideslip: it may be noted in Fig. 1 that the vanes are placed in a plane where the diameter of the fuselage crosssection is equal to five times the dimensions of the vanes.

Device A, which in itself did constitute a considerable advance, nevertheless had serious flaws.

1.2. Device B

Device B, described below, was designed especially for spin, in such a way that the anemometer is able to give continuous and

sufficiently accurate information on the speed vector throughout the range traversed. Some of the information given is even redundant, at least within a certain range of incidence and slip.

1.2.1. Operative Principles

The operative principles of this anemometer are based on simultaneous knowledge of data from one rod -- neighboring probe to one Chaffois device -- and the distribution of parietal pressures around the circumference of a cross section of the forward part of the fuselage. The rod is normal to the cross section considered.

The rod (Fig. 4) was equipped with a total pressure intake and a static pressure intake with four openings; this number was raised to 12 during calibration, for reasons which will be shown later.

The pressure distribution within the cross section of the fuselage is determined by a ring with 12 parietal pressure intakes (Fig. 5). Behind each intake is a capsule with an electrical outlet. These pressures are in opposition to the static pressures at the rod; the same is true for the total pressure at the rod.

In flight, all data from the ring and the rod are transmitted by radio to a computer for immediate processing.

Although the values supplied by this anemometer make it possible to define the speed vector totally, by completely covering the spin range α - β , nevertheless the quantities to be determined first are not α and β , but two other angles which are more directly accessible with the device studied and are defined below.

In Fig. 6, angle d is defined as the dihedral angle formed by the plane of symmetry PS of the aircraft and the plane

PV containing the axis of the fuselage and the direction of the wind.

In plane PV, the direction of the wind and the longitudinal axis form an angle c .

Pair $c - d$ is equivalent to $\alpha - \beta$.

$$\alpha = \tan \text{arc} (\tan c \cdot \cos d)$$

$$\beta = \sin \text{arc} (\sin c \cdot \sin d)$$

As will be seen later, the ring furnishes the value of maximum parietal pressure within its plane, as well as the angle of position d for this pressure. Comparison of the maximum pressure with the data given by the rod furnishes angle c .

The device was calibrated in the IMF Lille 2.40 m wind tunnel. Two mock-ups of a single long-fuselage aircraft were used. These were in turn mounted on a special support making it possible to vary the incidence from 0° to 90° and the sideslip from -90° to 90° by slight movements of the center of the mock-up.

The rod was studied in full scale, mounted on a forward fuselage tip. The parietal pressures on the ring were read during simulated spin.

1.2.2. Information Furnished by Rod

Figure 7a shows, as a function of angles c and d , the ratio $K_s = (P_r - P_s)/(\rho U^2/2)$, where P_r = static pressure at rod, P_s = static pressure of wind tunnel, $\rho U^2/2$ = kinetic pressure of wind tunnel,

This graph refers to a rod equipped with a static pressure gauge with four openings. It may be noted in this graph that with a constant angle c , ratio K_s varies widely: the static

pressure at the rod is not isotropic.

In order to improve exploitation of the anemometric results, the tests were performed again using a static pressure gauge with 12 openings (see Fig. 4). The results are given in Fig. 7b, which shows that this time the static pressure curve for the rod has become isotropic: no irregularities can be detected in the curves. Since angle d no longer comes into play, it was possible to represent the curves given in Fig. 7b solely as a function of angle c: see Fig. 7c.

The total pressure curve for the rod also being isotropic, these results are given in Fig. 7d, in which the ratio

$$K_c = \frac{P_t - P_r}{\frac{1}{2} \rho U^2}$$

is plotted as a function of angle c, P_t being the total pressure for the rod and P_r being the static pressure for the rod.

By way of example these same results were transferred to Fig. 7e, but as a function of angles α and β . It may be noted that the same values for K_c may be given for different pairs α, β . The same would be true for K_s .

On the basis of this observation, the choice was made to study c and d first rather than α and β .

1.2.3. Information Furnished by Ring

Figure 8 gives as examples two typical curves representing pressure distribution on the ring. The ratio K_p defined by:

$$K_p = \frac{P_t - P_r}{\frac{1}{2} \rho U^2}$$

is plotted as a function of angle d , P_g being the local pressure on the ring.

For pair α, β , Fig. 8b shows two curves which are asymmetrical to direction $d = 45^\circ$. The existence of these two curves is related to the existence of asymmetric flows which will be discussed in the chapter dealing with analysis of yawing moment.

The present section is reserved solely for study of the maximum value for local pressure -- $P_{g\max}$ -- within the plane of the ring, and thus the maximum value for K_p , termed $K_{p\max}$; this value was found to be very little affected by the asymmetry of the curve.

Several methods were tested in an attempt to determine $K_{p\max}$ and its direction d , some using overall characterizations for curve $K_p = f(d)$, and others using local characterizations.

(a) Overall methods

a.1. Method of least squares

This method does not always yield satisfactory results due to the asymmetry of the downwind flow. at certain values for angle c (see example given in Fig. 8b).

a.2. Method of ellipse of inertia

This method involves knowing the direction of the principal axes of inertia of the curve $K_p = f(d)$.

Here again, the method fails due to the asymmetry downwind for certain values for angle c .

a.3. Method of Spline functions passing through 12 measurement points

Computations using Spline functions passing through 12 points require approximately 2 seconds for the computer at the

In-Flight Testing Center where the aircraft spin tests took place; this interval is too slow for operation in real time.

Furthermore, when curve $K_p = f(d)$ is "wasp-waisted," /9
deformation of the Spline functions is such that the results sought are no longer accurate.

(b) Local methods

b.1. Cubic method

Four consecutive points are considered; an exact cubic curve is made to pass through these points and its maximum and direction are noted.

One point is then removed; an exact cubic curve is again made to pass through the points and the new maximum and direction are noted.

This operation is performed 12 times around the entire ring.

The highest maximum and its direction are retained.

This determination procedure was found to be much faster than the preceding (100 times faster). However, the precision of the maximum retained and its direction is slightly lower with this procedure.

b.2. Procedure based on comparison of values

The computer considers three consecutive points on the curve $K_p = f(d)$ and computes the sum of the three readings.

One point is then removed and a sum of three values is again computed.

This operation is performed 12 times.

The group of three points giving the maximum sum is retained, and the point immediately on each side of this group is added to it. The group of five points thus defined can then be characterized by a curve whose maximum will be determined. This system of five points is shielded from any angular area and thus from any source of ambiguity. Choice was made to pass a Spline function through these five points, which easily yields the maximum parietal pressure P_{lmax} and the corresponding angle d .

This was the procedure retained, due to the speed of computation and the quality of the results.

1.2.4. Utilization of Measurements

/10

The position of the maximum and its value can always be determined, no matter what the pressure involved may be. Thus with regard to aircraft, one no longer considers the coefficient K_p , but rather K'_p defined by:

$$K'_p = \frac{P_l - P_r}{P_t - P_r}$$

In the same manner, one has:

$$K'_{p \max} = \frac{P_{lmax} - P_r}{P_t - P_r}$$

The relationship between K'_p and K_p is given by:

$$K'_p = \frac{K_p - K_s}{K_c}$$

(see definition of K_s and K_c above).

Figure 9 shows the isotropic curves $K'_{p \max}$ as a function of angles c and d . This representation shows the ring to be very

slightly anisotropic; based on the tests, this can be attributed to the influence of the part of the aircraft to the rear of the ring.

Drawn from Fig. 9, where $d = 0$, Fig. 10 shows the variations in $K'_{p \max}$ as a function of c . Determination of $K'_{p \max}$ makes it possible to determine c . In order to take into account the anisotropy which was just mentioned, the value found is corrected as a function of itself and of angle d . The correction is zero when d is less than 50° . When d ranges from 50 to 90° , the correction is linear.

Figure 11 shows the maximum correction Δc (when $d = 90^\circ$) to be made in the value c obtained.

In practice, this correction, which remains slight, is made only when the sideslip is very considerable.

In summary, the procedure for utilization of the anemometer is as follows:

One first determines $K'_{p \max}$ and its direction d ; then on the basis of $K'_{p \max}$ it is possible to compute angle c , which is corrected on the basis of the value obtained for it and that obtained for d ; once the corrected c factor and d factor are known, it is possible to determine α , β and $\rho U^2/2$.

1.2.5. Remarks

/11

The value for c makes it possible to compute coefficients K_s and K_c :

K_s for determination of the real static pressure,

K_c for the real total pressure.

The real static pressure thus being known, there are two possible solutions for computation of the real air density: either by reference to the standard atmosphere or by consulting the temperature and static pressure recorded during the ascent of the aircraft.

The K_c value thus makes it possible to compute the speed.

1.2.6. Vanes

Experience gained in the use of anemometric device A (1.1) has resulted in the vanes of the anemometer B being placed much farther forward on the nose so that they will be less protected from the wind at the high α or β factors attainable.

An incident vane is located on the left side of the nose and a sideslip vane beneath the nose, which in this case is preset $\pm 120^\circ$ on the axis of the nose so that it will retain its value at extremely high incident angles (see Fig. 12).

On the other hand, the arrow of the vane, the type conventionally used in aircraft testing, which heavily protected the stabilizers of the vane when the incident angle was between 0° and 30° , was replaced by another arrow which was much shorter (29 mm rather than 76) and denser in order to keep the weight of the vane in equilibrium (Fig. 13).

Designed in this way, the vanes were calibrated on the forward tip of the fuselage in full scale, as already mentioned, and equipped with the rod. The mV values given by their angular potentiometer were read. The α - β range of correct use of the vanes was thus defined; as Fig. 14 indicates, this range is:

$$\begin{array}{l} 0^\circ \leq \alpha \leq 90^\circ \\ -30^\circ \leq \beta \leq +30^\circ \end{array}$$

Beyond 30° sideslip, the incident vane is protected by the nose; below -30° , its sensitivity to sideslip is negligible, and the values given by the potentiometer are thus too close to each other to be used. /12

1.2.7. Full-Scale Tests

Anemometer B was tested on a fighter airplane during its series of spin tests.

Although the anemometer and the vanes could be compared only within a relatively narrow α - β range, this is nevertheless extremely valuable in defining the degree of accuracy of the information furnished by the anemometer.

The tests performed showed the information furnished by the anemometer to be extremely useful in the exploitation of spin recordings. Within the range where they may be compared, the values given by the vanes and by the anemometer for α and β are extremely close, as shown by Fig. 15. This agreement makes it possible to conclude that α and β have been extremely accurately determined within the entire range -90° to $+90^\circ$ of these two angles.

Thus dorsal spin is as well defined as ventral spin.

2. Measurement of Yawing Moment

2.1. Preliminary Remarks

Spin by long-nosed fighter aircraft is frequently erratic. By means of vertical wind tunnel tests it is possible to show that in many cases the nature of the spin may be very appreciably modified by the overall shape of the forward part of the fuselage or by detailed design changes in this forward part. In wind tunnel tests it was also found that the reproducibility of spins

by the aircraft concerned was very slight, with the result that virtual statistical analyses were necessary, with the necessity of repeating some tests a large number of times. Conventional measurements of yawing moment were performed on the mock-ups used in a spin wind tunnel, first in order to obtain the additional information necessary for insight into the phenomena involved, and second, to be able to devise means of correcting these phenomena, including safety devices.

2.2. Example of Yawing Moment at Zero Sideslip

At zero sideslip, the yawing moment was found to be extremely high at some incident angles for some types of long-nosed fighter aircraft. The absolute value of the yawing moment is not defined, but this factor is given by its ratio to the yawing moment furnished at zero α and β by the rudder when it is deflected downward; it was found that this ratio may equal 3. /13

An initial reaction to this type of result is the conclusion either that the airflow in the wind tunnel is not axial or that the mock-up is not symmetrical.

Figure 17 shows the variations in the curve for 10° sideslip: these results eliminate the error due to sideslip.

In response to the second point, the tests were performed again with the nose -- which was a cone of revolution -- turned on a length equal to 67% of the mean chord of the aircraft.

Figure 18 gives the results obtained for four positions 90° from each other. These results eliminate the error of symmetry for the mock-up.

It was thus necessary to acknowledge that these results, even though surprising, corresponded to a real phenomenon, considering the fact that highly asymmetrical airflow can occur around a body such as an aircraft of the type studied, placed in symmetrical positions in relation to the speed at a distance. Furthermore, it was shown that the direction of asymmetry is determined by very slight unevenness or deformations in the forward tip of the fuselage.

Our American colleagues have noted identical phenomena.

This asymmetry in airflow may explain some observations made during free spins, dealing on the one hand with the problems involved in voluntarily reproducing this type of phenomenon and, on the other, with certain movements detrimental to recovery from spin.

The horizontal wind tunnel tests were followed by various modifications in the shape of the mock-up for the purpose of making the airflow symmetrical.

2.3. Criteria for Classification of Modifications

To be able to determine which of the modifications studied constituted the most effective means of correcting the airflow, two criteria were set up to facilitate comparison.

2.3.1. Criterion of Symmetrization

/14

This was based only on results obtained at zero sideslip, and defined the efficiency of the modification made in the nose with regard to symmetrization of the airflow.

In Fig. 19, the term a characterizes the decrease in the maximum modulus of yawing moment C_n ; term b characterizes the gain in α over the entire range (beginning with $\alpha = 0$) where

C_n remains relatively low; and term e characterizes the decrease over the entire range where C_n is high.

The criterion is $K_1 = ae/b$. The farther this value is below 1, the more efficient the device.

2.3.2. Criterion of Stabilization

This concerns measurements made with sideslip at values other than zero and defines the range of yawing stability, that is, the α - β range within which the yawing moment tends to decrease sideslip.

This second criterion is also composed of three terms (Fig. 20):

- term f characterizing the increase, at $\beta = 0$, in the extent of the α range (beginning with $\alpha = 0$) where $C_{n\beta}$ retains its sign;
- term g characterizes the increase in the average value of $C_{n\beta}$ within the preceding range;
- term h characterizes the increase in the average extent of β in the α - β range (beginning with $\alpha = \beta = 0$) where $C_{n\beta}$ remains of the same sign.














The criterion is $K_2 = f \cdot g \cdot h$. The greater this value is than 1, the more efficient the device.

2.4. Modifications of Nose

Tests using nose configurations derived from basic geometry and of extremely diverse types, both realistic and unrealistic, were performed with the objective of first defining the types of modifications which would be most efficient in producing a symmetrical airflow.

The following are the results of this phase of research:

/14'

<u>Modifications :</u>		<u>K₁</u>	<u>K₂</u>
Basic geometry		1	1
Ring perpendicular to axis of nose			0.75
Small fins at extreme forward tip			1,6 (detrimental)
"Screwdriver" nose		0.45 0.06	
Rounded nose		0.45	
Conical end fitting		0.80	
Vertical surface above nose		0.9	
Keel		1.2	
Striated nose		0.6 to 1	
Flat, rectangular or trapezoidal strakes, either sawtoothed or in the form of crenellations			0.005 to 0.04 9

Measurements for the criterion K_2 of stabilization were performed only for configurations having met criterion K_1 of symmetrization; these were various types of strakes for which K_2 remained very close to 9.

2.5. Effect of Strakes on Yawing Moment

/15

Free spin tests for both criteria showed strakes to be the design of preference.

Figure 21 gives the ratio of the yawing moment obtained at zero sideslip with a nose equipped with strakes to the yawing moment given at zero α and β by the rudder deflected downward. This ratio was appreciably lower than that obtained with the original nose. The maximums are approximately one-tenth their former values; the flow is almost symmetrical.

Figure 22, with the same frame of reference (downward direction, zero α and β) gives the yawing moment as a function of sideslip for a characteristic incidence (40°) with and without strakes. It shows that the range of stability has increased (see the definition of this range in 2.3.2).

Finally, Fig. 23 gives the range of α - β stability with the original nose and with the same nose equipped with strakes.

2.6. Relationships Between Yawing Moment and Anemometric Measurements

Measurements determined by anemometry, which were discussed in Chapter 1, give some information on the way in which the very significant C_n factors which have just been considered are obtained at $\beta = 0$.

As was stated in Section 1.2.3, due to the asymmetry of the upstream airflow, with the use of the anemometer only those pressure intakes in the ring producing a separation point of the airflow at that structure were taken into account.

Since the method for exploitation of results had not been predetermined, an attempt was made to determine fine variations in parietal pressure. For this purpose, the ring of the mock-up was equipped with 18 pressure intakes (every 20°). In addition, the forward part of the mock-up fuselage containing the ring was a cone of revolution formed by metal worked on a lathe with the ability to rotate around its axis. Thus by turning the nose to positions at intervals of 5° it was possible to determine the parietal pressure every 5° in four manipulations.

An initial exploitation of the measurements was made by plotting, for a single α - β pair, the four curves passing through /16 the four groups of 18 points separated by intervals of 5° . Although neighboring curves were generally obtained, on the other hand for some α - β pairs, especially those for which α was between 25° and 45° , it was found that the four curves for a single α - β combination could differ appreciably from each other.

Thus for a single α - β pair, one notes with reference to the example given Fig. 8b:

- that the curves are not symmetrical in themselves: this implies that the airflow has no plane of symmetry;
- that, on the other hand, the different curves are symmetrical to each other in relation to the direction d defined by $K_{p \max}$ (see Section 1.2.3).

Since the asymmetrical airflow may occur in one direction or the other, the asymmetry thus is not due to a defect in the mock-up, but to an intrinsic characteristic of the airflow (metastable flow), which seems to be linked to certain values for angle c ($30^\circ < c < 60^\circ$) as defined in Section 1.2.1.

With the aircraft itself, equipped with anemometric device B (see 1.2), a metastable asymmetrical airflow may be recognized by

considering the parietal pressure on the ring and plotting its polar curve $P_{\theta} = f(\theta)$. The pressure integral around the circumference of the ring indicates the direction and orientation of the force collected on the nose.

3. Safety Devices

3.1. Preliminary Remarks

It has always been understood that an aircraft cannot be used in in-flight spin tests until wind tunnel tests have first shown, first, that the spin is not too severe in itself, and second, that the recovery from spin can be carried out under acceptable conditions. However, safety devices have been studied, and the present chapter discusses some aspects of these studies.

3.2. Parachutes

/17

3.2.1. Principles of Utilization

An "antispin" parachute is sometimes considered for use in recovery from spin. It was demonstrated some time ago that in order to be effective, and often merely so as not to be dangerous, the antispin parachute should meet certain conditions: it should have a long cable, on the order of 1.5 times the length of the aircraft; the canopy should have a wide surface area; the point of attachment should be such that when extended, the cable does not rub against or become caught on a component of the aircraft. Under such conditions, the parachute, outside areas of extremely disturbed flow, should be able to provide a means of recovery. However, one should consider the case of extremely agitated spins, which virtually preclude the use of antispin parachutes due to the high risk of the cable becoming caught on the aircraft.

For this type of spin, another means of using a recovery parachute has been devised. In this case the parachute is termed a "loss-of-control" parachute, meaning that it must be

used at a very early stage, even before the spin is actually established; this type of use presents a definite problem in regard to the extremely short time left for the pilot to decide to use the parachute. However, it was not our purpose to consider this aspect, but only the aerodynamic aspects. This type of parachute would not be specialized for spin only, but rather could also be used as the braking parachute for the aircraft; thus it is not necessary for the parachute cable to meet the requirements of the antispin parachute, and its limits of utilization can thus be studied more precisely.

3.2.2. Results of Wind Tunnel Parachute Tests

Figure 24 shows the limit of utilization of the parachute as a function of α and β , based on its behavior for four cable lengths which were whole multiples of a characteristic cable length for a braking parachute equalling approximately 35% of the length of the fuselage.

It was found that the α - β range of satisfactory parachute operation was too small with the use both of the cable length of a braking parachute and twice this length, for these lengths to be considered usable.

When the length used is three times that of the characteristic length of a braking parachute cable, utilization of the loss of control parachute extends over virtually the entire α - β range; a small residual danger zone remains, however, for very high incident angles at zero sideslip; the canopy opens correctly, but the cable comes into contact with the stabilizers.

In order to define the filling of the parachute within the possible utilization range, the ratio of the tension within the cable to that which would be obtained in the airflow at a distance

was formed. Figure 25 shows, as a function of α - β , the limit of the range where the ratio obtained falls to one third for the four cable lengths: a rapid increase was noted except for the longest lengths, at a very high α value and $\beta = 0$.

In spin tests of a parachute one actually seeks to determine the introduction of a moment which in the present case is a pitch moment, the parachute cable always being located in a direction fairly close to that of the speed at a distance.

Thus Fig. 26 gives the ratio of the pitch moment due to the parachute to the centrifugal pitch moment as a function of the incidence, for cable lengths equal to and twice that of a braking parachute cable and a rotation speed of one rotation every 2.5 seconds. It may be seen that this ratio is always less than 1, or remains too close to 1.0. The same would not be true of a cable length at least three times that of a braking parachute cable.

In conclusion, in order to be efficient and reliable, the loss-of-control parachute should have characteristics very close to those of the antispin parachute. It is not likely that it will be possible to use braking parachutes for this purpose.

3.3. Auxiliary Surfaces

When it is found necessary to modify the phenomena occurring during wind tunnel spin tests while the structure of the aircraft must be kept the same, the frequent solution is to add external surfaces which become means of recovery if they are retractable. It has been our usual policy for some time to recommend such procedures to aircraft manufacturers; the auxiliary surfaces have frequently been implanted at the rear of the fuselage, and the

earliest example of this type of structure in fixed form was produced by Fouga Magister (1953); in a number of cases manufacturers have designed these structures in retractable form. Auxiliary structures are also located under the fuselage and toward the front, the earliest example of this type of design being produced by Durandal (1955). More recently, the strakes discussed in Chapter 2.5 have been studied. Two types of fighter aircraft have been equipped with these structures to provide means of recovery. During in-flight testing of one of these aircraft, the efficiency of the structure itself was studied without the necessity of using it as a means of recovery. The results obtained checked out very closely with the predicted results for the wind tunnel.

3.4. Rockets

3.4.1. Preliminary Remarks

Rockets also may be considered as recovery devices. Their use was studied for light aircraft in full-scale spin tests; the purpose was to provide a device which could easily be incorporated into any spin test installation for this type of aircraft. Thus there was reason to optimize the implantation and dimensions of such rockets. Tests were performed in a vertical wind tunnel on mock-ups of light planes equipped with small rocket engines.

The control of spin does not deal with forces but with moments; thus the tests were conducted by introducing effects separately around three axes. In equipping the mock-up, the amount of weight which had to be placed on board in order to cover a wide range of thrust required that the combustion chamber be close to the center of inertia; extremely lightweight tubes are used for connection with the nozzles; the efficiency is very low. Other design configurations may be used for aircraft and the efficiency will be considerably improved.

3.4.2. Results

The tests were made primarily for the types of spin which are most difficult to control, that is, flat spin (angle of incidence close to 90°) and fast spin (≤ 2 seconds/airplane rotation).

In the following, the thrust values are given as a percentage of the weight of the aircraft and the periods of operation of the engine are given as the average length of time for one spin rotation. See Fig. 27 for the points of implantation of the rockets.

3.4.2.1. Rocket Influencing Pitch

/20

From the outset this means of recovery is more attractive than a "yaw" or "roll" rocket since a single pitch rocket installation will be adequate, no matter what the direction of spin may be.

The tests performed revealed that unfortunately the effect of a rocket influencing pitch is highly inadequate. In order to obtain acceptable recovery without the aid of the rudders, it is necessary to attain an unrealistic level of thrust and specific impulse: the thrust must be greater than the weight of the aircraft if one wishes to obtain an effect within approximately one rotation.

3.4.2.2. Rocket Influencing Yaw

With a rocket influencing yaw, obviously operating in an opposite direction to that of rotation, the thrust moduli necessary are much lower than those required for pitch.

With the mock-ups studied, artificially restricted to flat, rapid spin, even though the rudders were kept in operation during

spin, rapid recovery was obtained with levels of thrust equal to 20 and 12% of the weight of the aircraft exerted during one and two rotations respectively.

The same results were again obtained with a level of thrust 5% of the weight of the aircraft exerted for three rotations, if the rudders were kept in neutral position at the same time.

Figure 28 gives a few examples of variations in longitudinal attitude with the application of yawing moment and, by way of comparison, the results obtained by placing the rudders in neutral position.

3.4.2.3. Rocket Influencing Roll

Both directions of action must be considered with regard to rockets influencing roll.

If the operating wing is defined as the wing located on the outside of a turn in the same direction as the spin, the rocket may tend either to lower or raise the operating wing.

A few results obtained during flat rapid spin are given in the table below. The levels of thrust are characterized by their modulus as percentage of the weight of the aircraft and by their length of occurrence in number of rotations. Recovery, when it is obtained, is given in rotations. /21

3.4.2.4. Comparison of Results Obtained Around Three Axes

In Fig. 29 we have gathered a few characteristic results obtained with rockets acting around each of three axes. The levels of thrust which it was necessary to apply until recovery was obtained are given as a function of the length of time necessary for recovery. Since the specific impulse determines

Thrust		7% - 3.4 rotations	18% - 2.5 rotations	22% - 3.7 rotations
Rocket raising operating wing	Rudders left in pro-spin position	Change in spin	Change in spin	2 rotations
		Spin not very steep	Steep spin	
	Rudders placed in in neutral position	3.4 rotations	2.5 rotations	
Rocket lowering operating wing, rudders left in pro-spin position			Change in spin Spin not steep	3 rotations

the weight of the rocket, while the thrust may determine the structural implantation, iso-specific impulse curves are also plotted in this figure. The left-hand part of the figure represents a comparison of yaw and roll, and the right-hand part reproduces a scale which is small enough so that it is possible to include a point representing pitch. The increasing order of efficiency was found to be: pitch, roll, yaw. This increase may be characterized by applying to the three cases the coefficients $1/15$, $1/5$ and 1 .

It should be noted, however, that for yaw two rockets or one adjustable nozzle are necessary; for roll, beyond a given level of specific impulse recovery may be obtained no matter what the direction of force may be, while on the other hand the attitudes assumed may not always be favorable to purity of movement. The tests on rolling moment have not been completed, and it appears that the preferential direction of action

may change depending on the nature of the spin. If the yawing action is used, it may be noted that a relatively small rocket can provide a very efficient means of recovery: 4% of the weight of the aircraft acting simultaneously on the rudders should always permit recovery. By comparison, the drag produced by an antispin parachute in undisturbed airflow may be set at 50% of the weight of the aircraft, which leads to much lower efficiency.

3.4.3. Longitudinal Action of a Rocket

During the research whose principal results have just been discussed, a few tests were performed in which a longitudinal thrust was applied representing a level of thrust equal to 20% of the weight of the aircraft. No effect was noted, other than a slight modification of the relative positions of the aircraft and the axis of spin.

From this it may be concluded that the assumed traction produced by a propellor or thrust from a jet engine has only a negligible direct effect, the traction becoming slight due to the angle of incidence and the jet engines having a strong tendency to extinguish. If propellers do produce an effect, this should be sought in gyroscopic couple or in modification of the orientation of the wakes of the planes and the fuselage. This effect, which could be beneficial in one direction of spin, may on the other hand be unfavorable in the opposite direction, with the result that any aircraft should be able to show a capability for recovery from spin with its engine stopped or at least slowed down.

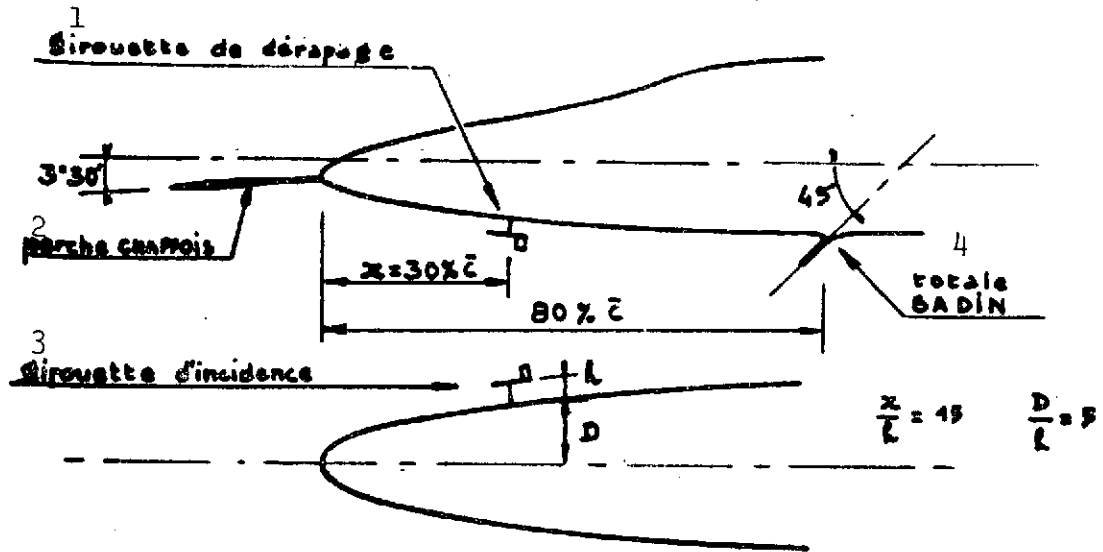


Fig. 1. Diagram of anemometric device A.

- Key:
- 1. Sideslip vane
 - 2. Chaffois rod
 - 3. Incident vane
 - 4. Badin total

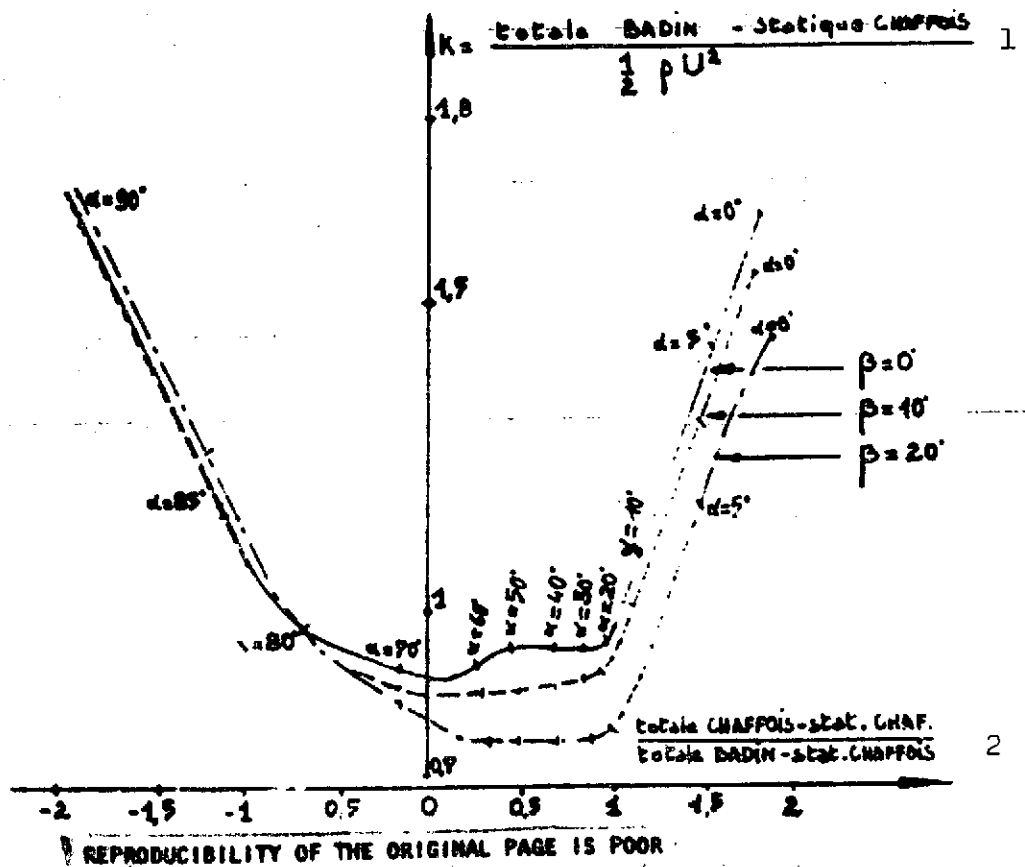
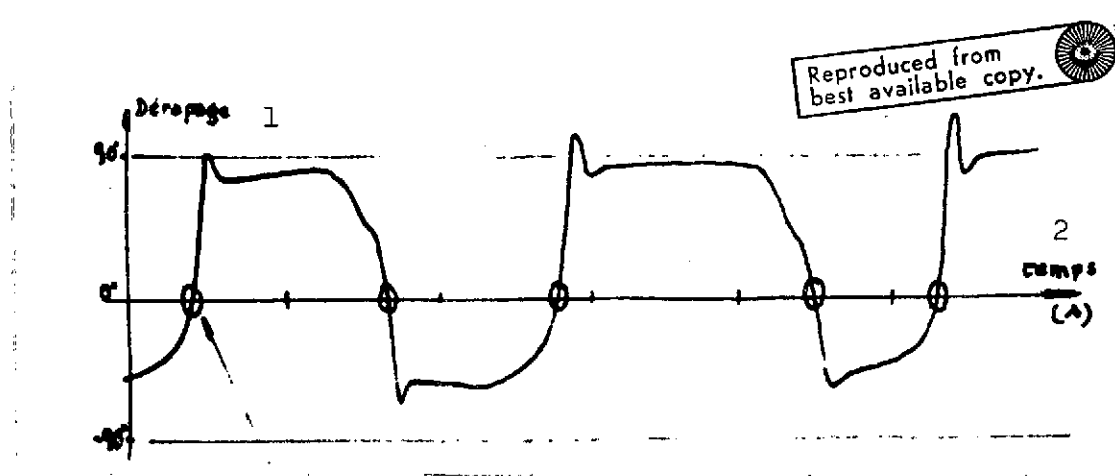


Fig. 2. Utilization curve for anemometer A.

- Key: 1. Badin total pressure gauge - Chaffois static pressure gauge
2. Chaffois total pressure gauge - Chaffois static pressure gauge
- Badin total pressure gauge - Chaffois static pressure gauge



Only points at which anemometer is usable for the type of spin considered.

Fig. 3. Readings from sideslip vane of device A((at high incidence).

Key: 1. Sideslip; 2. time

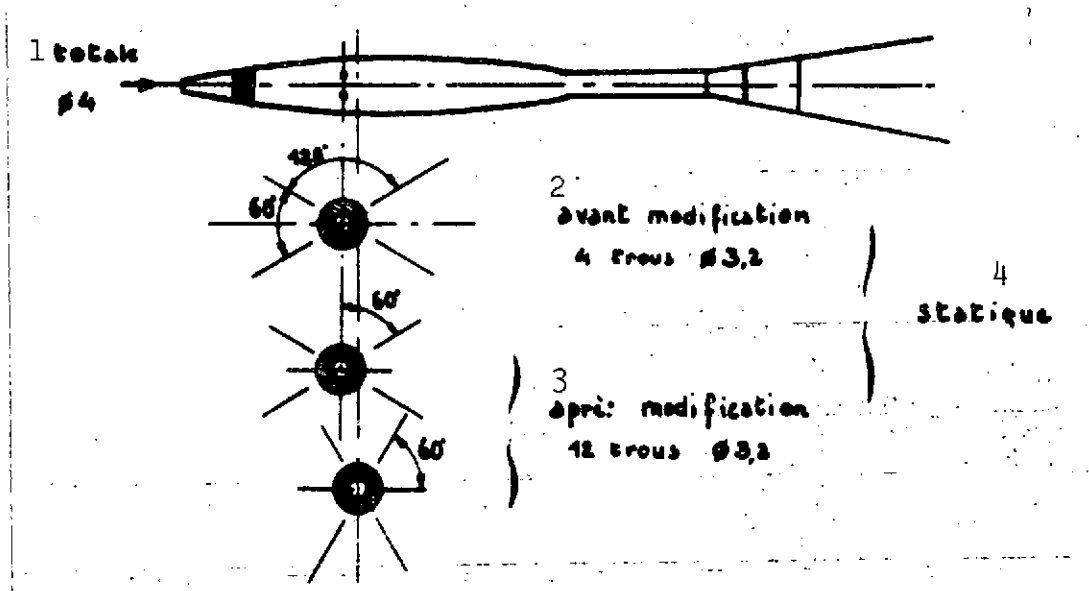


Fig. 4. Rod for anemometer B.

Key: 1. Total: diameter 4
2. Prior to modification: four openings, diameter 3.2
3. After modification: 12 openings, diameter 3.2
4. Static

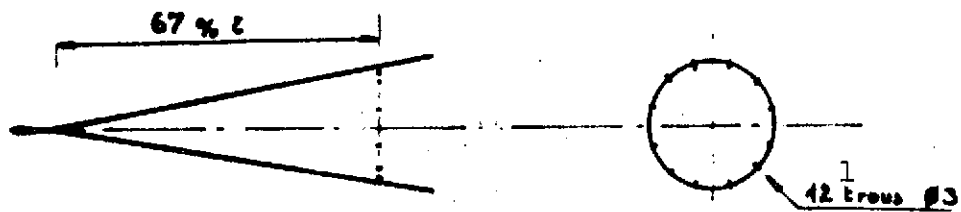


Fig. 5. Position of pressure ring of device B.

Key: 1. 12 openings, diameter 3

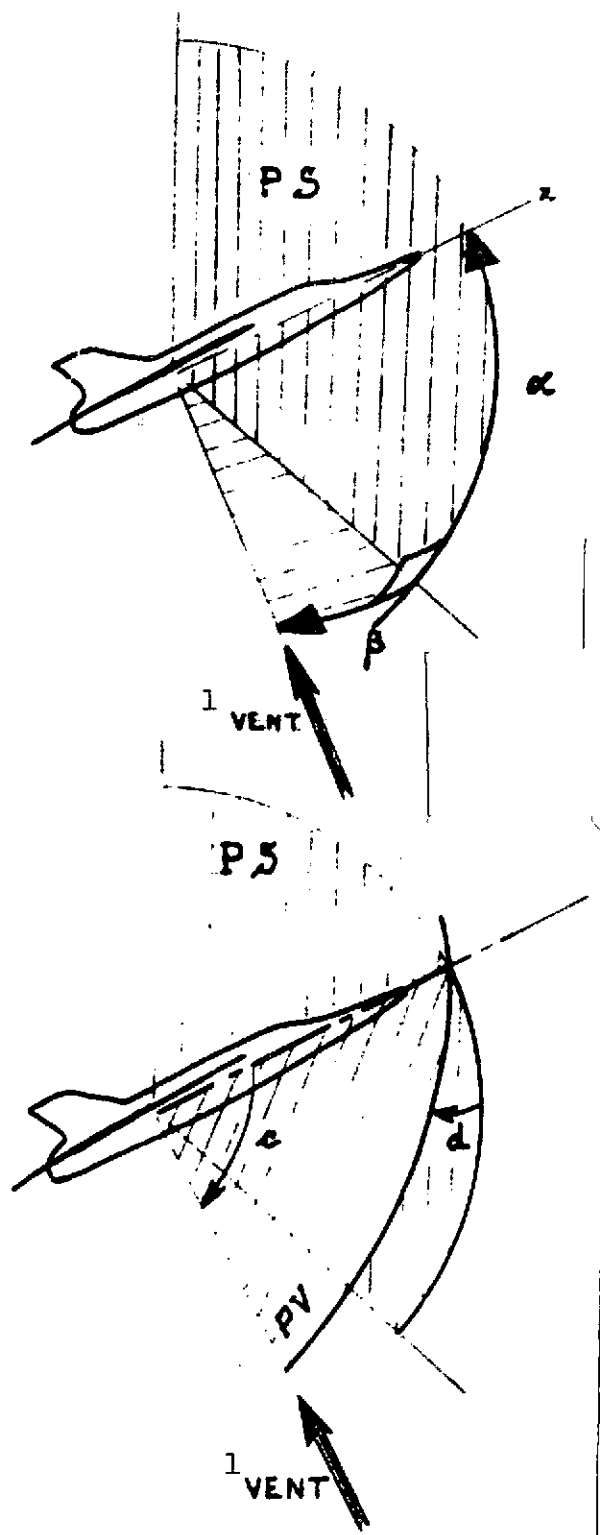


Fig. 6. Definition of anemometric angles c and d used in device B.

Key: 1. Wind

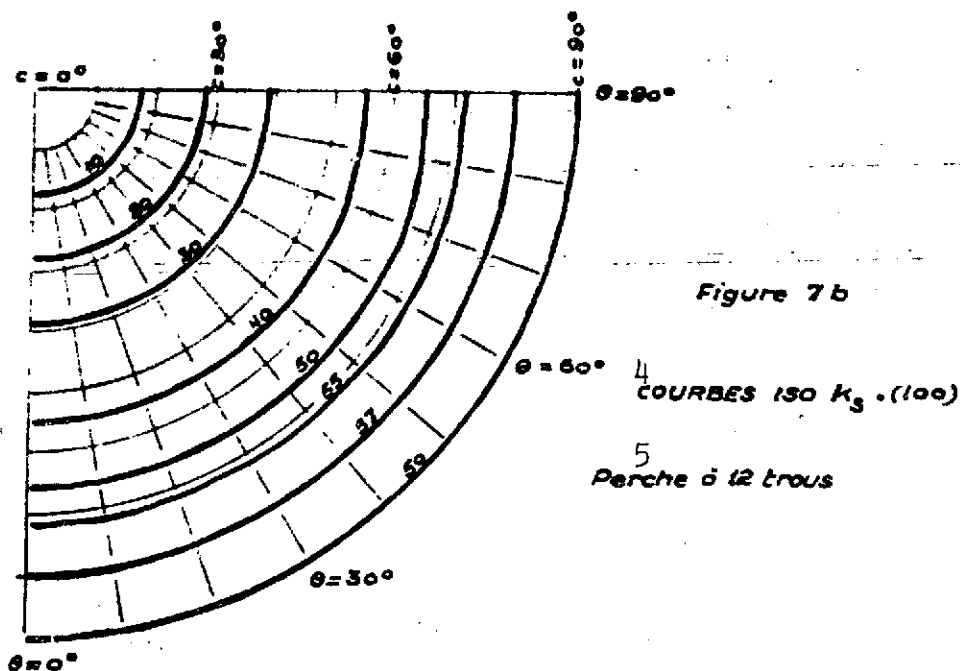
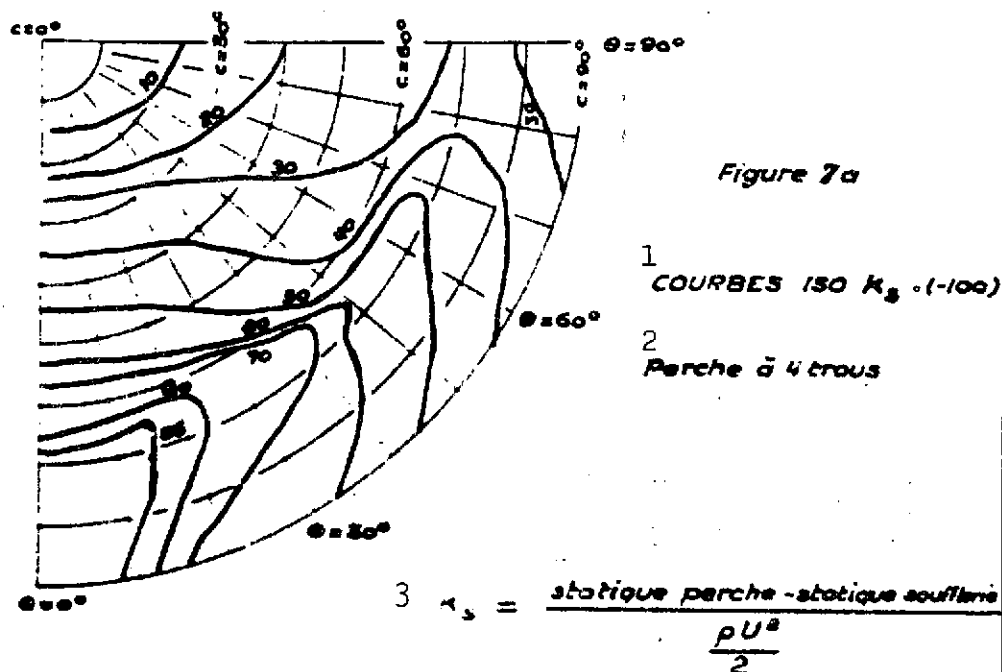


Fig. 7 a & b. Information given by rod B.

- Key:
1. Isotropic curves
 2. Rod with 4 openings
 3. Rod static pressure - wind tunnel static pressure
 4. Isotropic curves
 5. Rod with 12 openings

Note from Errata: In Figs. 7 a & b, read "d" for "theta".

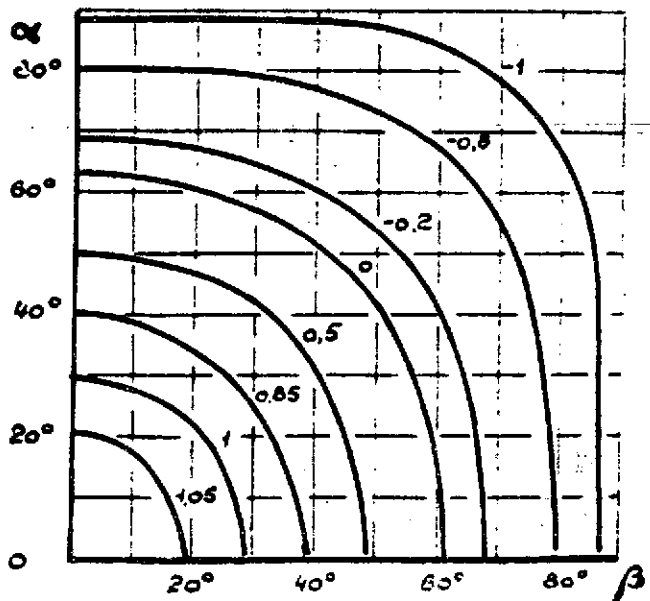
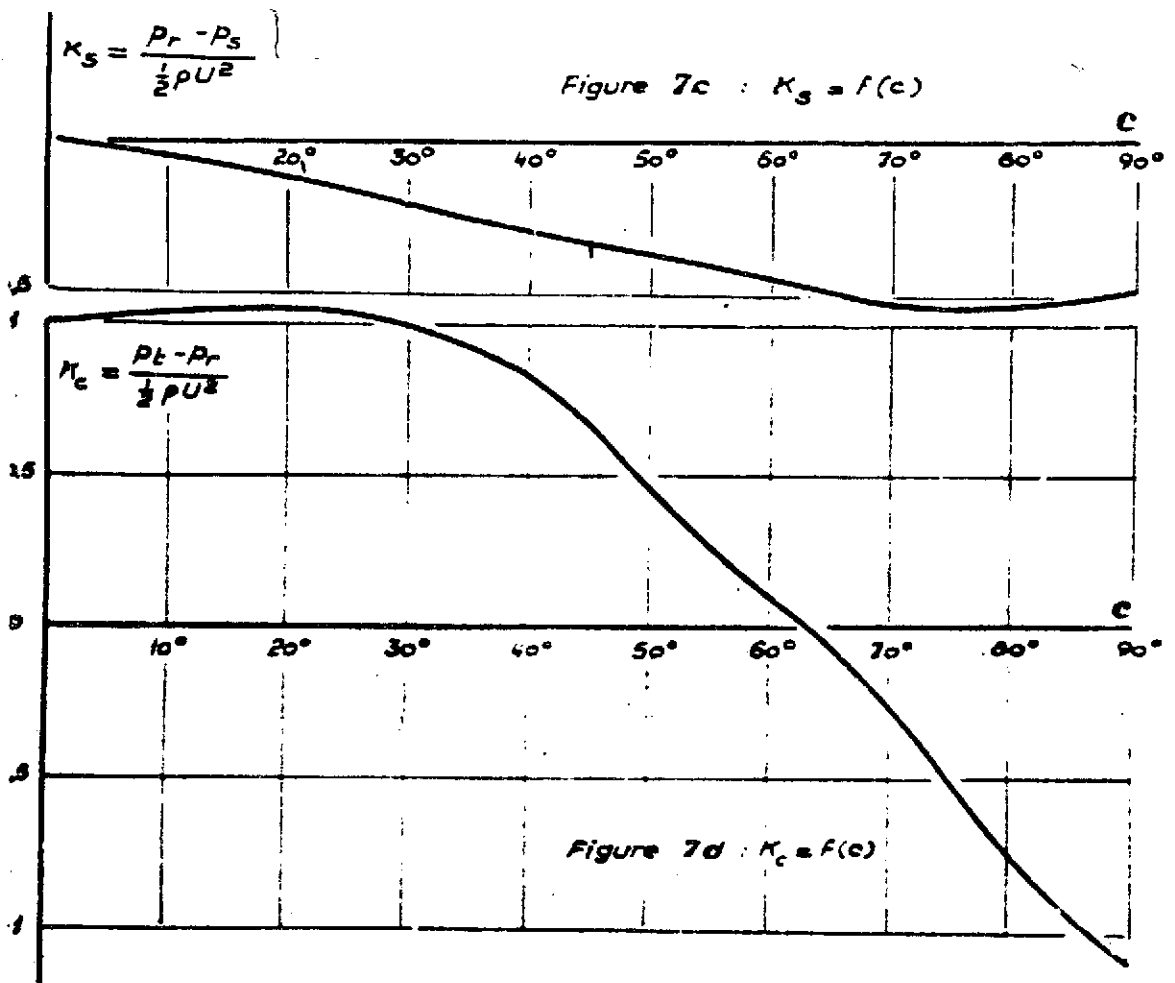


Figure 7e
1 Courbes d'iso K_C

Fig. 7 c, d, e. Information given by rod B (continued).

Key: 1. Isotropic curves

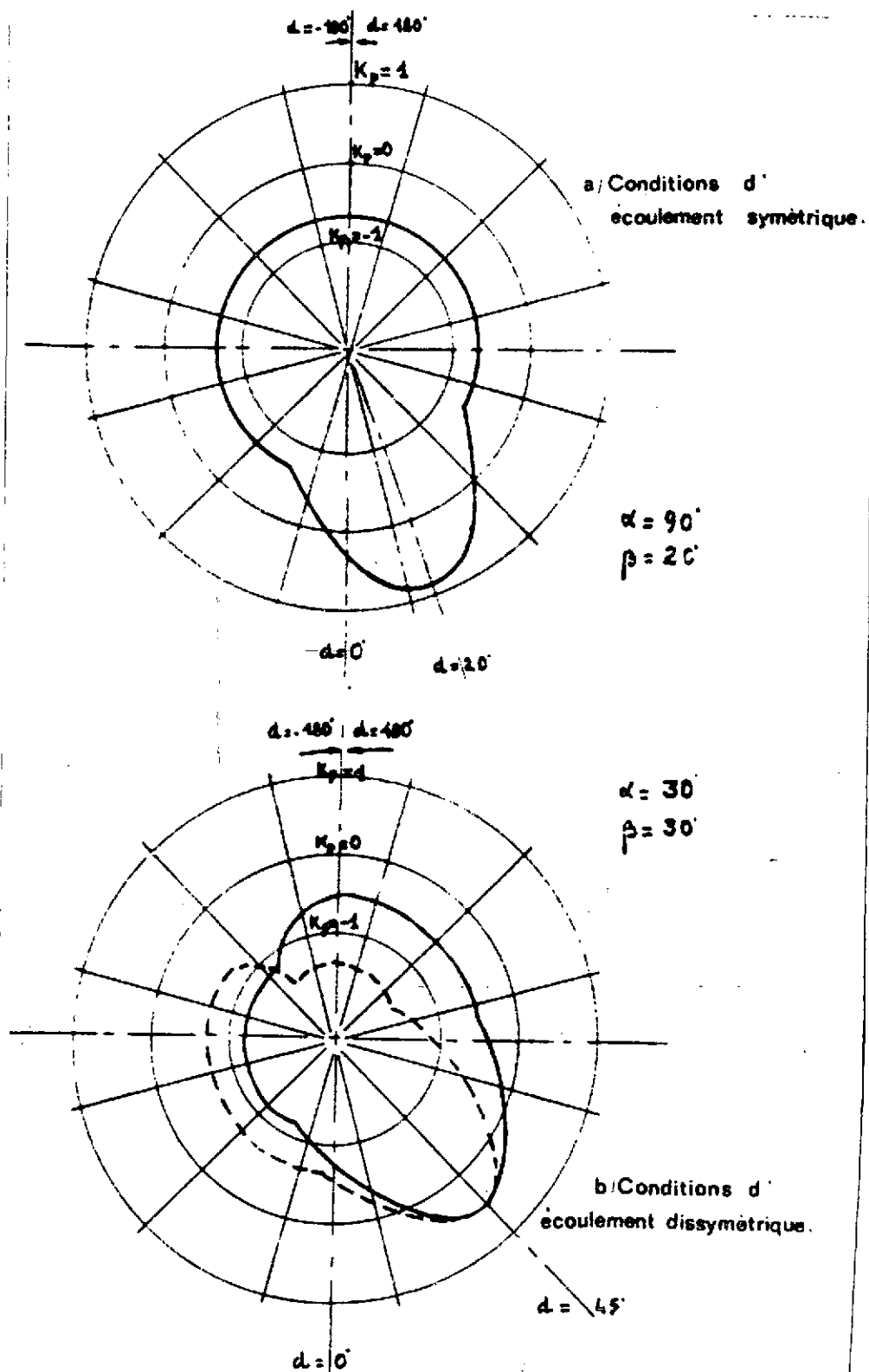


Fig. 8. Examples of pressure readings on the ring of device B.

- a. Symmetrical flow conditions
- b. Asymmetrical flow conditions

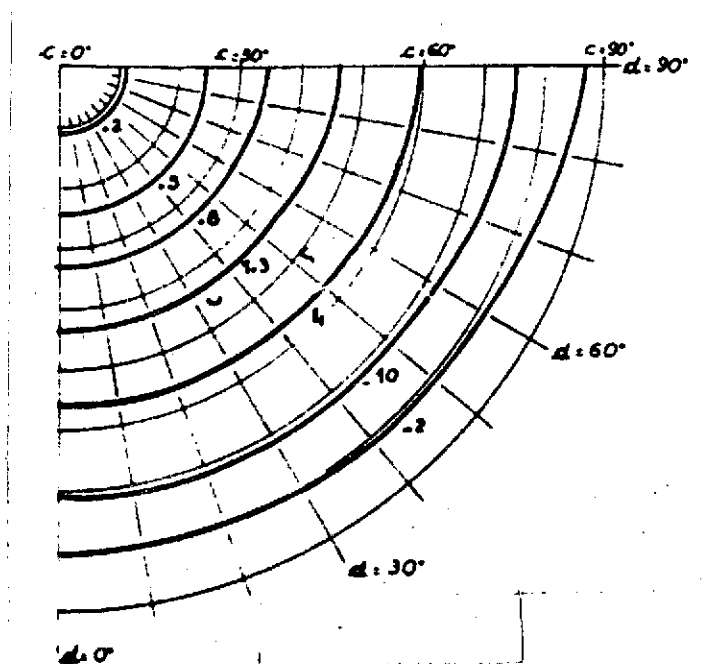


Fig. 9. Isotropic curves $Kp \text{ Max.} = \frac{p_{l \text{ max}} - p_r}{p_t - p^*}$

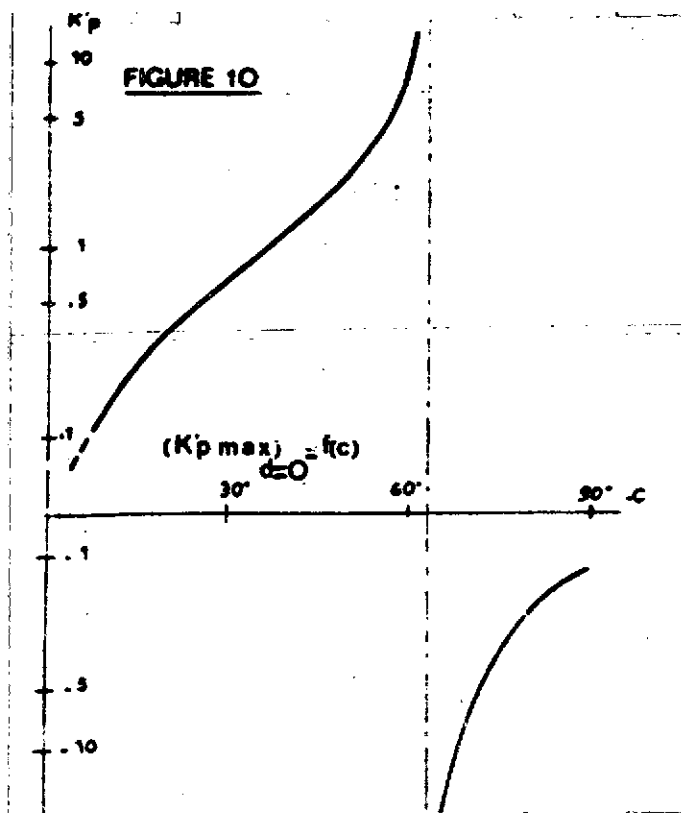


Fig. 10.

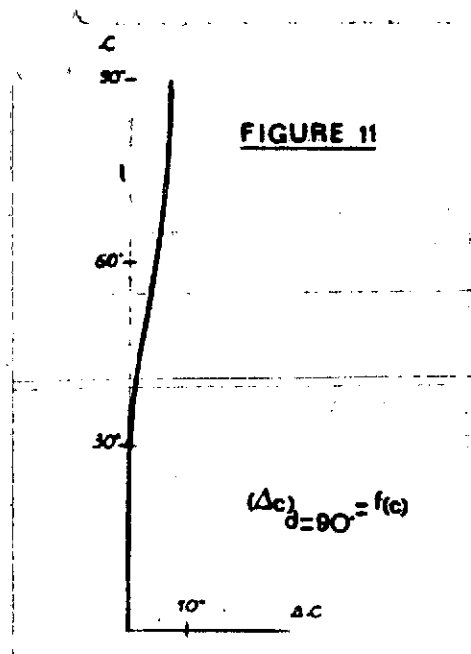
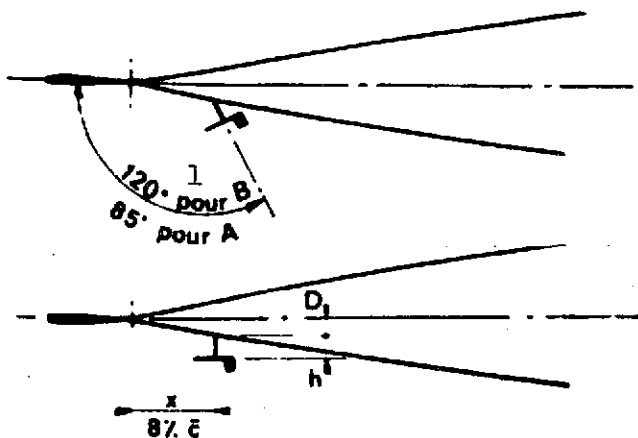


Fig. 11.



2 Dispositifs
anémométriques

	A	B
$\frac{x}{h} =$	15	3
$\frac{D}{h} =$	5	0.5

Fig. 12. Placement of vanes.

Key: 1. For
2. Anemometric devices

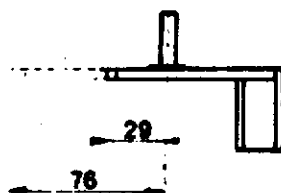


Fig. 13. Detail of vanes before and after modification.

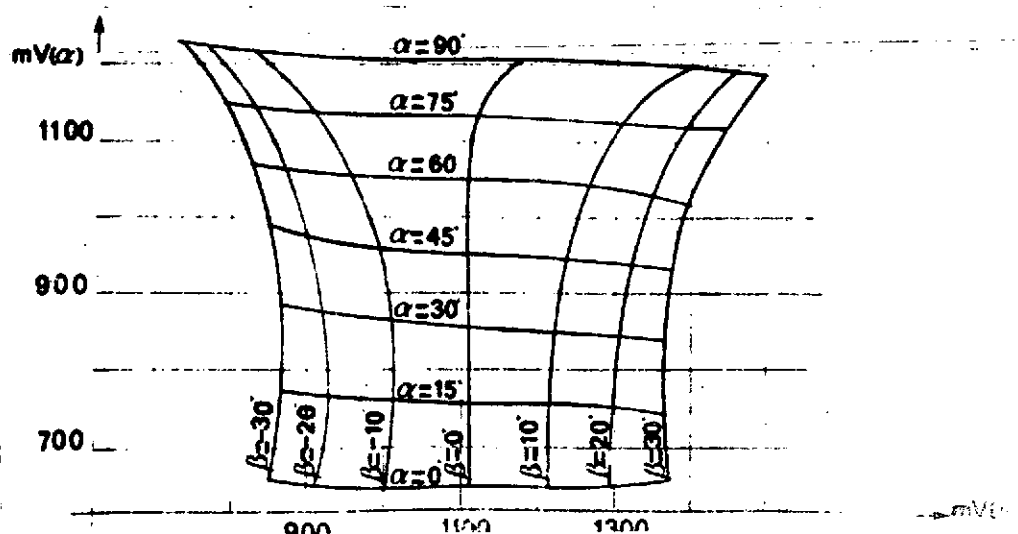


Fig. 14. Readings from vanes for B.

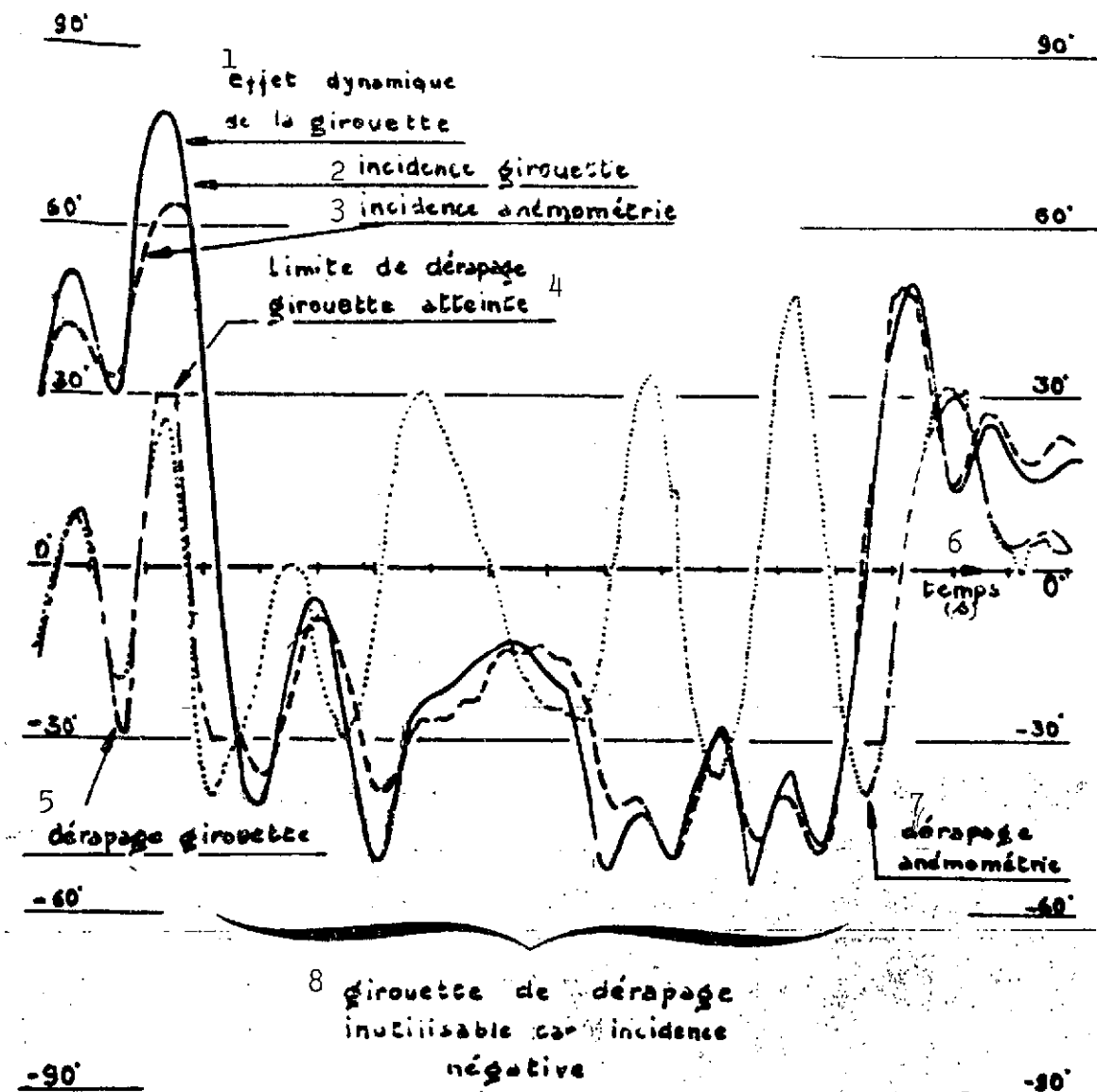


Fig. 15. Comparison of incidence and sideslip given by the vanes and the anemometer.

- Key:
1. Dynamic effect of vane
 2. Vane incidence
 3. Anemometer incidence
 4. Vane sideslip limit reached
 5. Vane sideslip
 6. Time
 7. Anemometer sideslip
 8. Sideslip vane unusable due to negative incidence

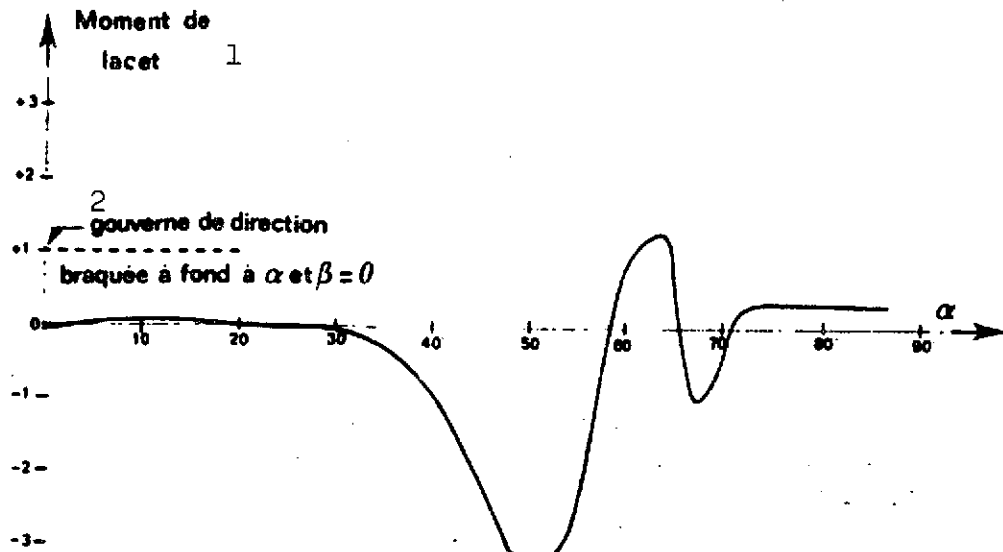


Fig. 16. Measurements of yawing moment: asymmetry of yawing moment at zero sideslip.

Key: 1. Yawing moment
2. Rudder deflected downward at ...

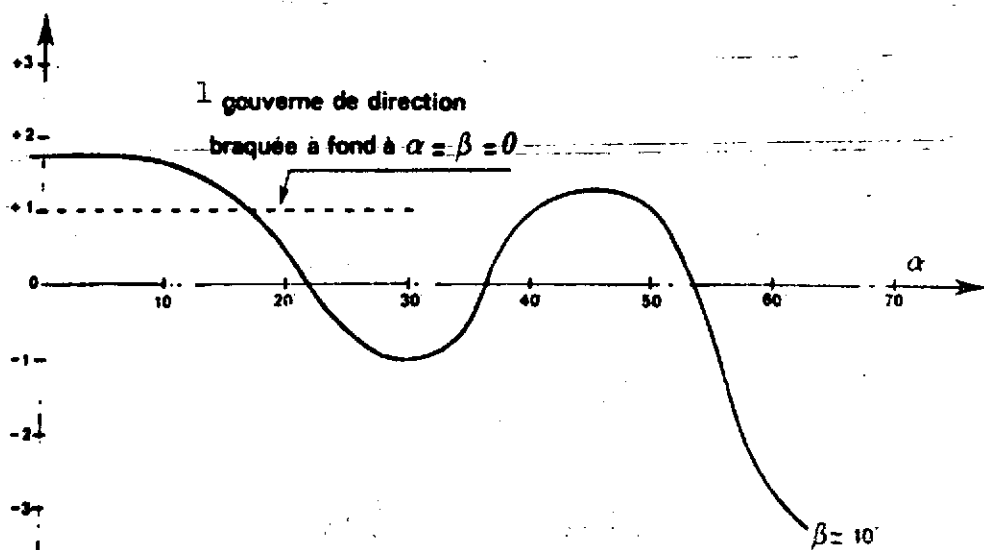


Fig. 17. Measurements of yawing moment: yawing moment at low sideslip.

Key: 1. Rudder deflected downward at ...

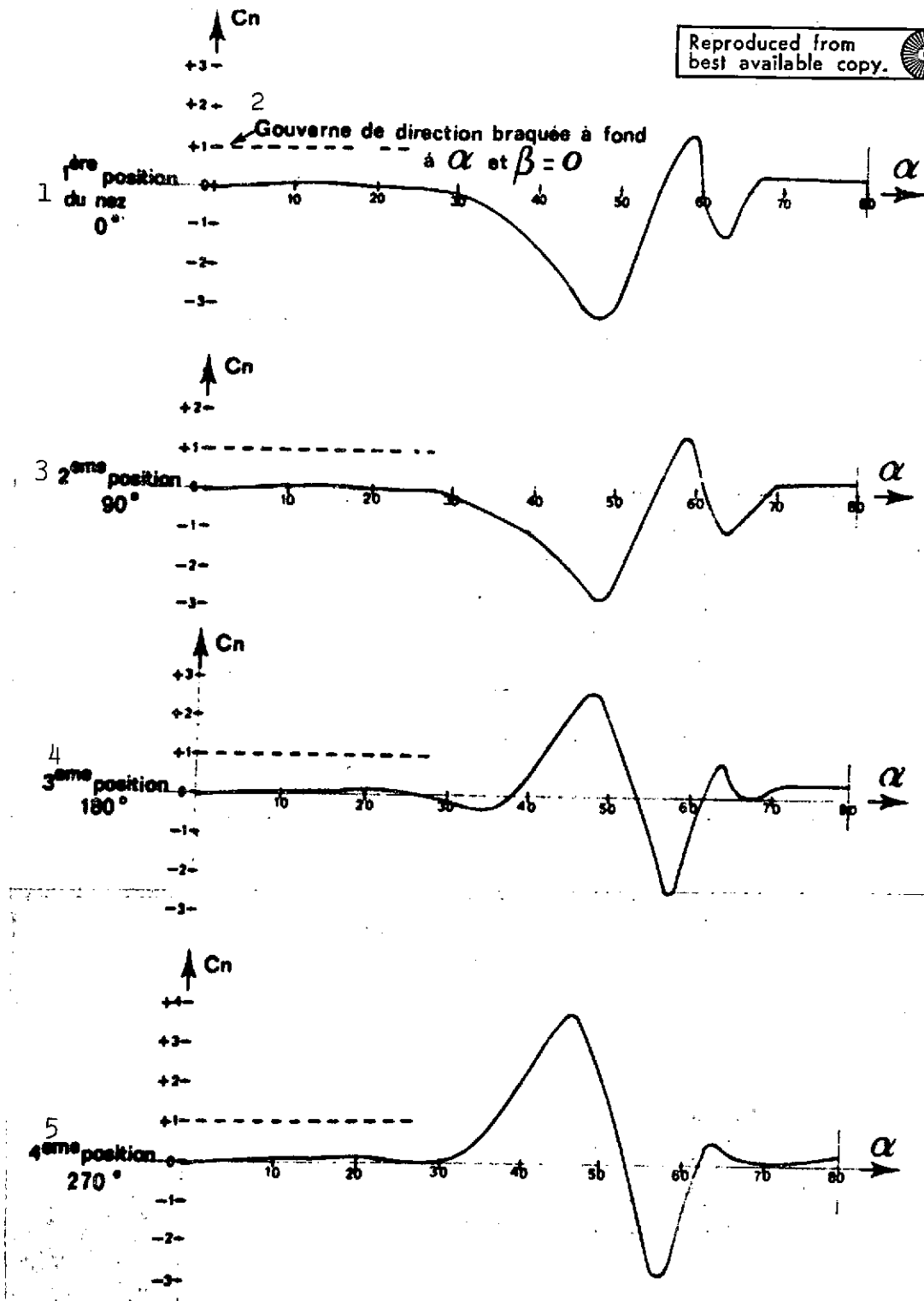


Fig. 18. Measurement of yawing moment at zero sideslip, with successive rotational positions of nose.

- Key: 1. First position of nose
 2. Rudder deflected downward at....
 3. Second position
 4. Third position
 5. Fourth position

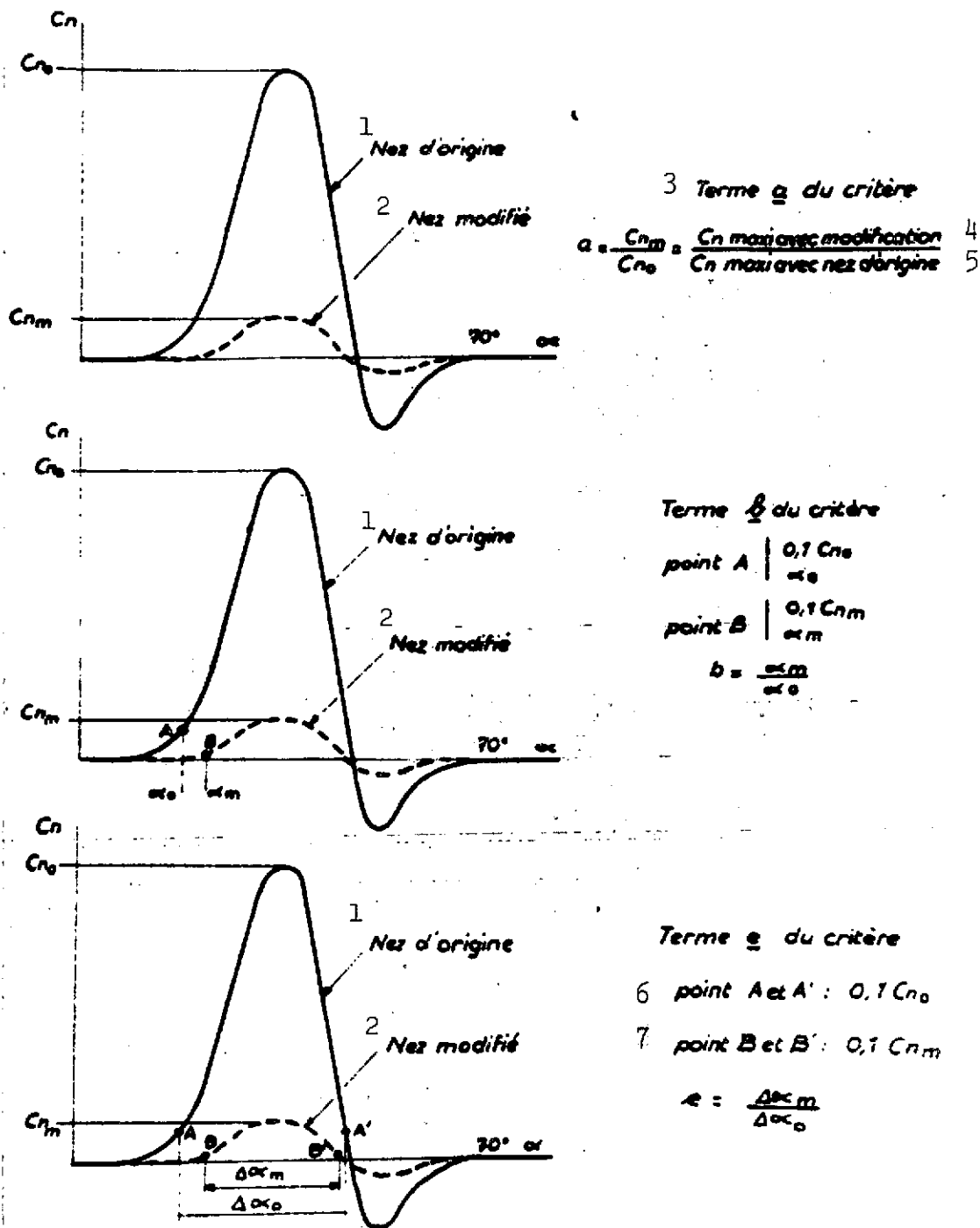


Fig. 18. Symmetrization criterion: K_1 (all at β); $K_1 = ae/b$.

- Key:
1. Original nose
 2. Modified nose
 3. Term... of criterion:
 4. Maximum C_n with modification
 5. Maximum C_n with original nose
 6. Point A and A'
 7. Point B and B'

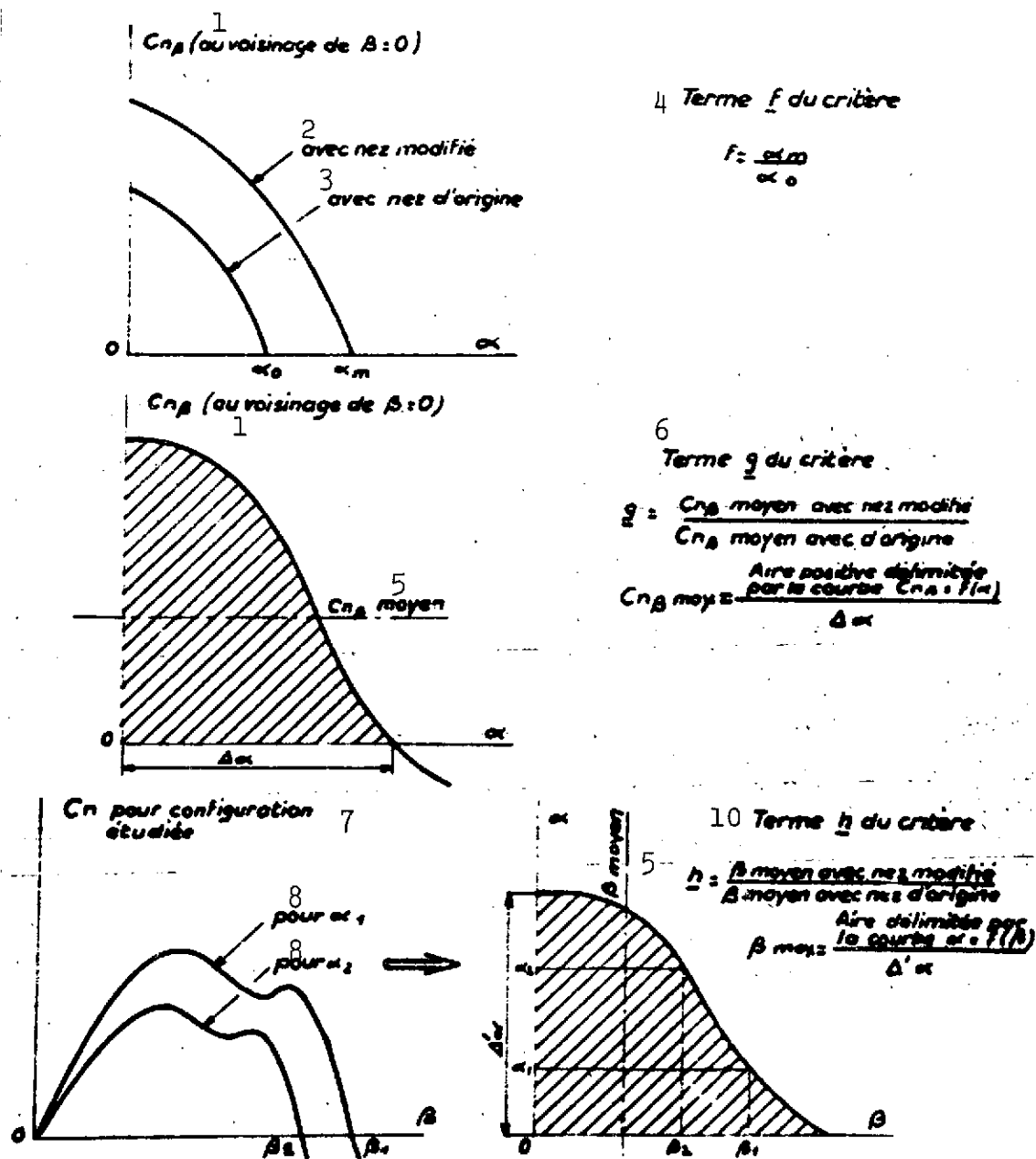


Fig. 20. Criterion of stabilization $K_2 = f \cdot g \cdot h$.

- Key:
1. In the vicinity of
 2. With modified nose
 3. With original nose
 4. Term f of criterion
 5. Mean
 6. Term g of criterion:
 $g = \frac{\text{mean } C_{n\beta} \text{ with modified nose}}{\text{mean } C_{n\beta} \text{ with original nose}}$
 - mean $C_{n\beta}$ = positive area delimited by curve ...

[Key continued on following page.]

Key to Fig. 20, cont'd:

7. C_n for configuration studied
8. For
9. Mean
10. Term h of criterion:
 $h = \text{mean } \beta \text{ with modified nose} / \text{mean } \beta \text{ with original nose}$
 $\text{maximum } \beta = \text{area delimited by the curve...}$

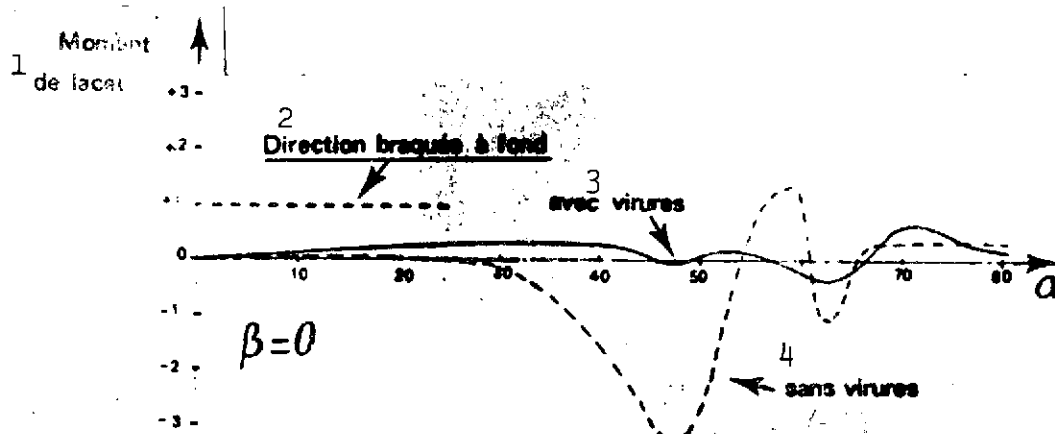


Fig. 21. Yawing moment with strakesbat at zero sideslip.

- Key:
1. Yawing moment
 2. Direction deflected downward
 3. With strakes
 4. Without strakes

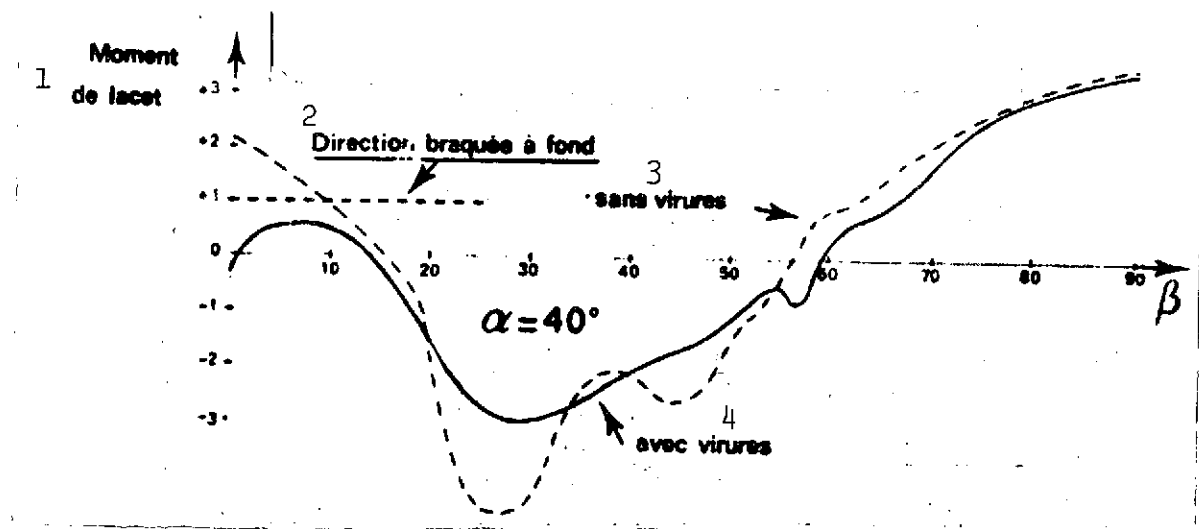


Fig. 22. Yawing moment with strakes at 40° incidence.

Key: Same as for Fig. 21.

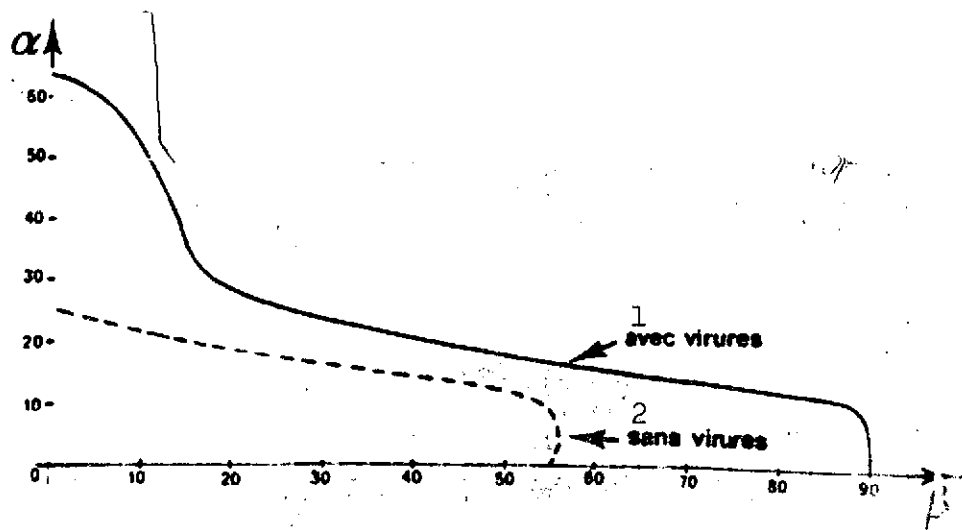


Fig. 23. Range of α - β stability within which yawing moment tends to produce a decrease in sideslip.

Key: 1. With strakes
2. Without strakes

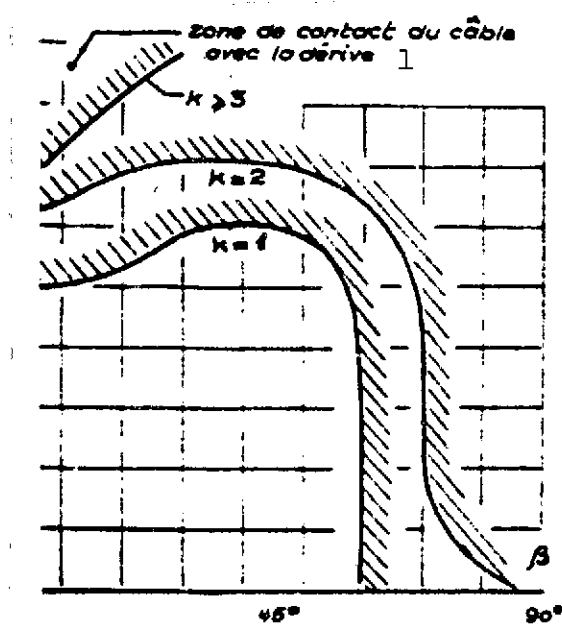


Fig. 24. Utilization limit of parachute on the basis of its behavior.

Key: 1. Contact area of cable with drift.

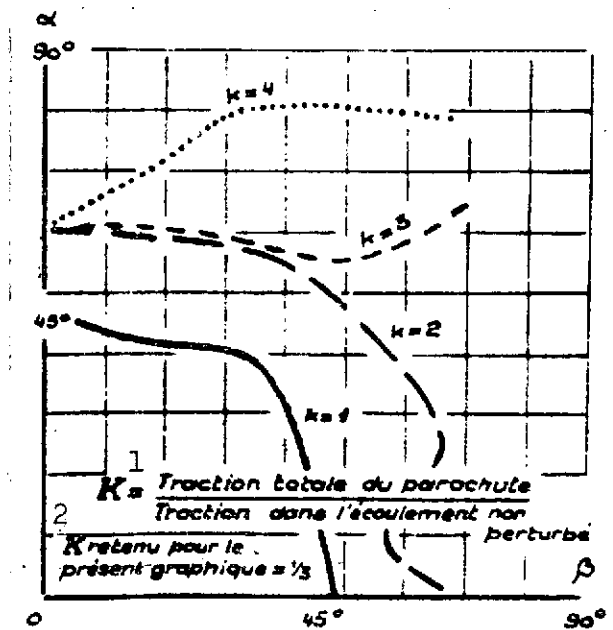


Fig. 25. Average stress in cable.

Key: 1. Total tension in parachute / tension in undisturbed airflow

2. K value used for this graph

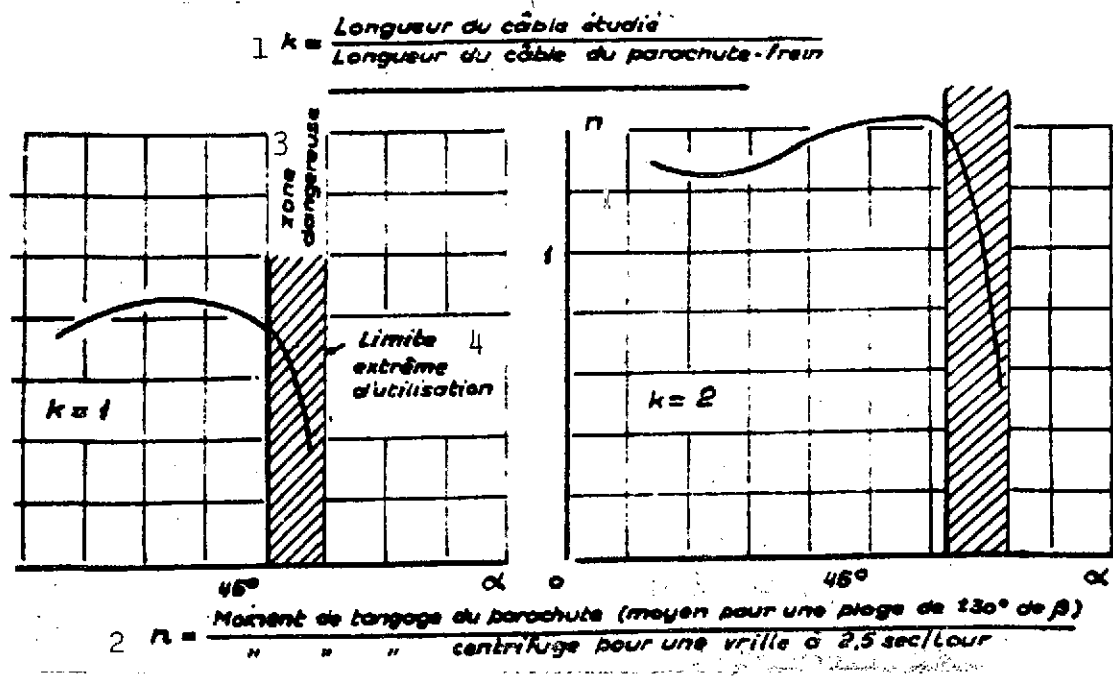


Fig. 26. Centrifugal couple of pitch balanced by parachute.

- Key: 1. Length of cable studied / length of braking parachute cable
2. Pitching moment of parachute (average for a range of 30° for β) / centrifugal pitching moment for spin at 2.5 sec/rotation
3. Danger zone
4. Extreme limit of utilization

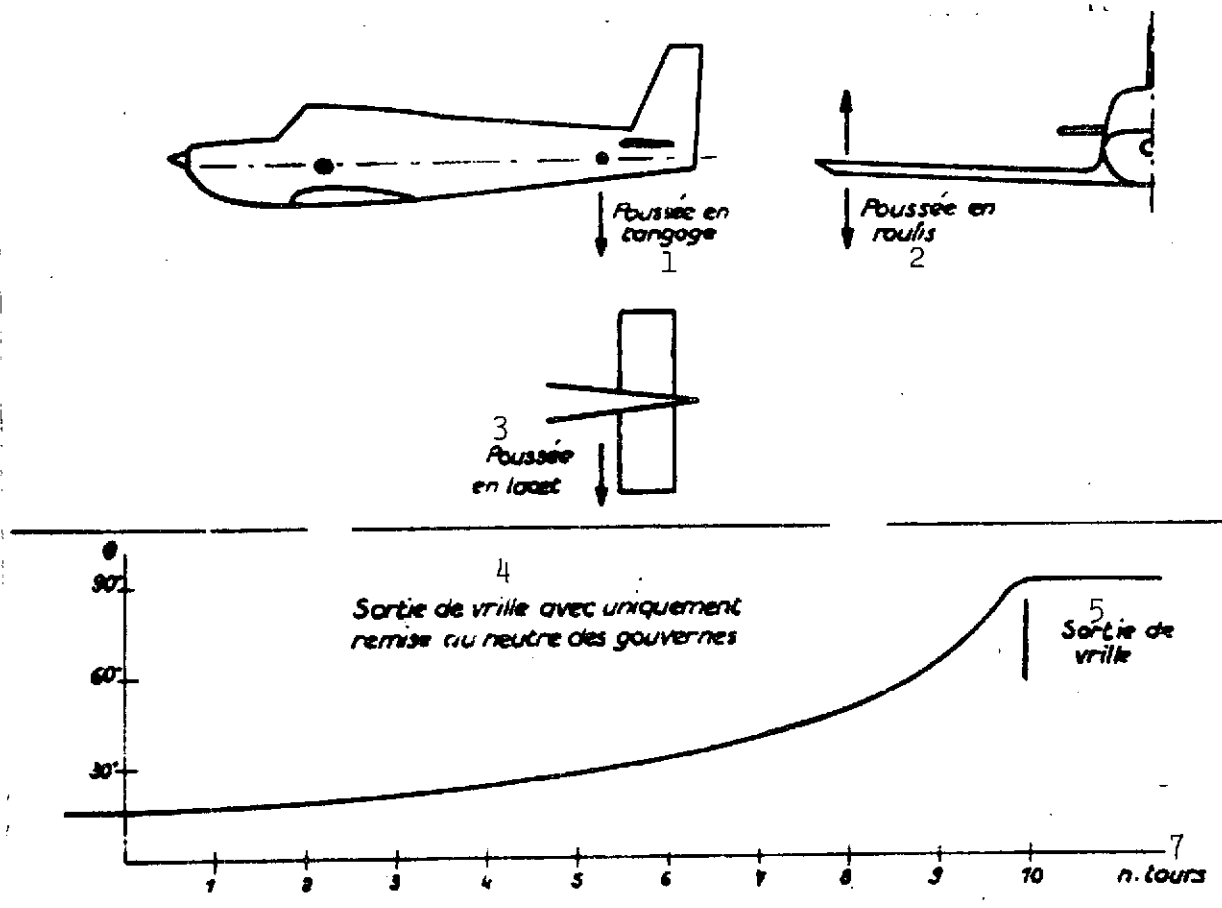


Fig. 27. Rocket engines: points of application of thrust.

- Key:
1. Pitching thrust
 2. Rolling thrust
 3. Yawing thrust
 4. Recovery from spin solely by placing rudders in neutral position
 5. Recovery from spin
 6. Diameter
 7. Rotations

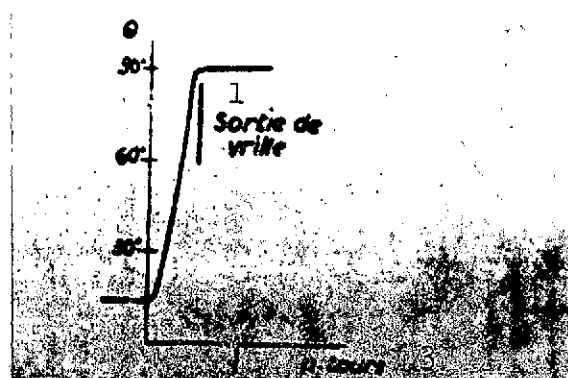
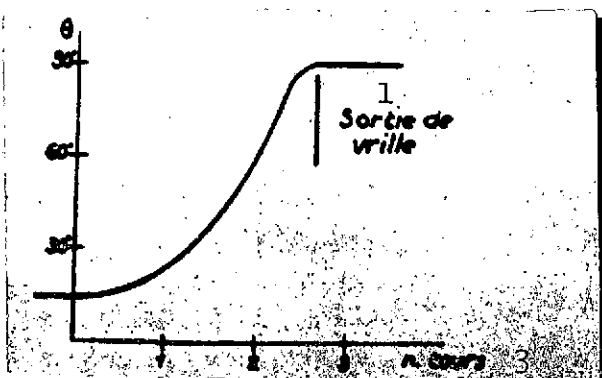


Fig. 28.

Recovery from spin with thrust 5% of weight of aircraft, influencing yaw, rudders in neutral position.

Recovery from spin with thrust 20% of weight of aircraft, influencing yaw, rudders remaining in pro-spin position.

Key: 1. Recovery from spin
2. Diameter
3. Number of rotations

Key to Fig. 29 (following page):

1. Thrust in newtons
2. Pitch
3. Roll
4. Yaw
5. Length of recovery in seconds
6. Iso-specific impulse curves: 1200 ns, 2400 ns, 4000 ns*
7. No recovery
8. Weight of aircraft
9. Curves
10. Thrust in: yaw
roll
pitch
yaw
11. Rudders
12. In neutral position
13. Kept in pro-spin position

*As corrected by Errata list.

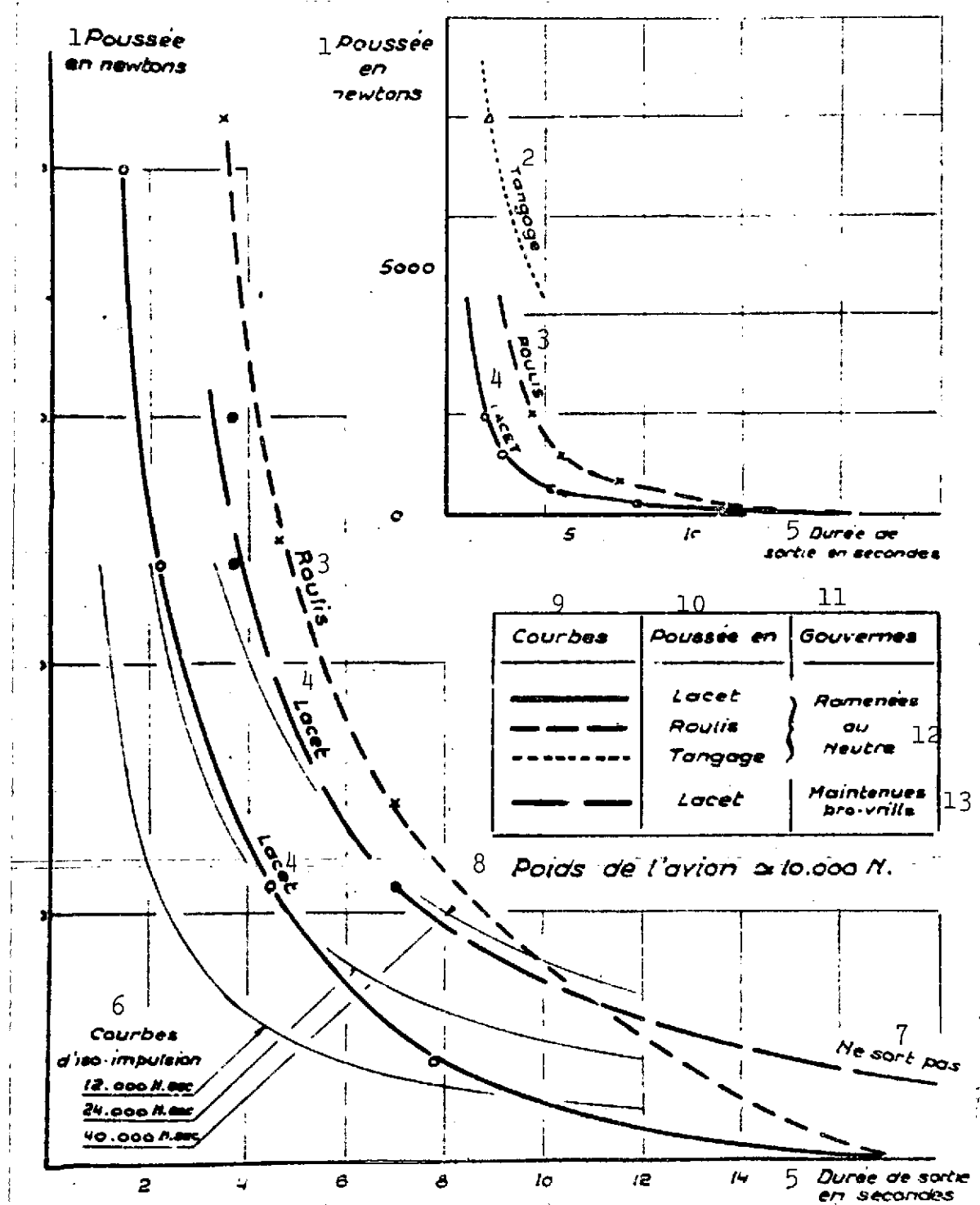


Fig. 29. Specific impulse: comparison of yaw, roll and pitch.